Carbonatation of [ethylene - glycidyl methacrylate]-based copolymers with carbon dioxide as reagent: from batch to solvent-free reactive extrusion

Bruno Guerdener,[a,b,c] Virgile Ayzac,[a] Sébastien Norsic,[a] Paul Besognet,[c] Véronique Bounor-Legaré,[b,*] Vincent Monteil,[a,*] Véronique Dufaud,[a,*] Jean Raynaud,[a,*] Yvan Chalamet[c,*]

[a] Univ. Lyon, CNRS, UMR 5128, Catalysis, Polymerization, Processes and Materials (CP2M), 43 Bd du 11 novembre 1918, Université Claude Bernard Lyon 1, CPE Lyon, F-69616 VILLEURBANNE, France.
vincent.monteil@univ-lyon1.fr ; veronique.dufaud@univ-lyon1.fr ; jean.raynaud@univ-lyon1.fr

[b] Univ Lyon, CNRS, UMR 5223, Ingénierie des Matériaux Polymères, Université Claude Bernard Lyon 1, INSA Lyon, Université Jean Monnet, F-69622 VILLEURBANNE, France.
veronique.bounor-legare@univ-lyon1.fr

[c] Univ Lyon, CNRS, UMR 5223, Ingénierie des Matériaux Polymères, Université Claude Bernard Lyon 1, INSA Lyon, Université Jean Monnet, F-42023 SAINT-ETIENNE cedex 2, France.
yvan.chalamet@univ-st-etienne.fr

# Supporting Information

Table of contents

# 1. Catalytic cycles for the carbonatation of epoxides

There are two routes for the carbonatation of epoxides with CO_2. The first one starts with the ring-opening of the epoxide by a nucleophilic catalyst derived essentially from halide anions of a Lewis-acidic cation (*e.g.* quaternary ammonium salts).[1] A selected Lewis (designed metal-based complexes)[2–14] or *Brønsted* acid (hydrogen bond organic donor)[15–19] activator A^+ could be used to synergistically activate the epoxide and stabilize the different intermediates (see **Scheme S1**).

The second route starts with the activation of CO_2 by steric hindered bases such as 1,5,7-triazabicyclo[4.4.0]dec-5-ene (TBD), 1,8-diazabicyclo(5.4.0)undec-7-ene (DBU) and/or nucleophiles presenting a delocalized negative charge such as BF_4^- or PF_6^- (see **Scheme S2**).[20–22] Bifunctional catalysts bearing both nucleophilic and acidic functionalities have also been developed, promoting hybrid mechanisms.[23–27]

In the first route, the nucleophile attacks the less hindered carbon atom of the epoxide **1**, to form the alkoxide anion **2** (**Scheme S1**, step **a**), which subsequently activates the CO_2 molecule to form the corresponding linear carbonate **3** (**Scheme S1**, step **b**). Finally, the cyclic carbonate **4** is formed by an intramolecular ring-closure, leading to the regeneration of the halide based catalyst (**Scheme S1**, step **c**).[1] In the second route, CO_2 is first activated by the catalyst, leading to the formation of the carboxylate intermediate **5** (**Scheme S2**, step **a'**). The less hindered carbon atom of the epoxide is then attacked by the carboxylate (**Scheme S2**, step **b'**) and an intramolecular ring-closure forms the cyclic carbonate **4** and regenerates the catalyst (**Scheme S2**, step **c'**).[21,22]
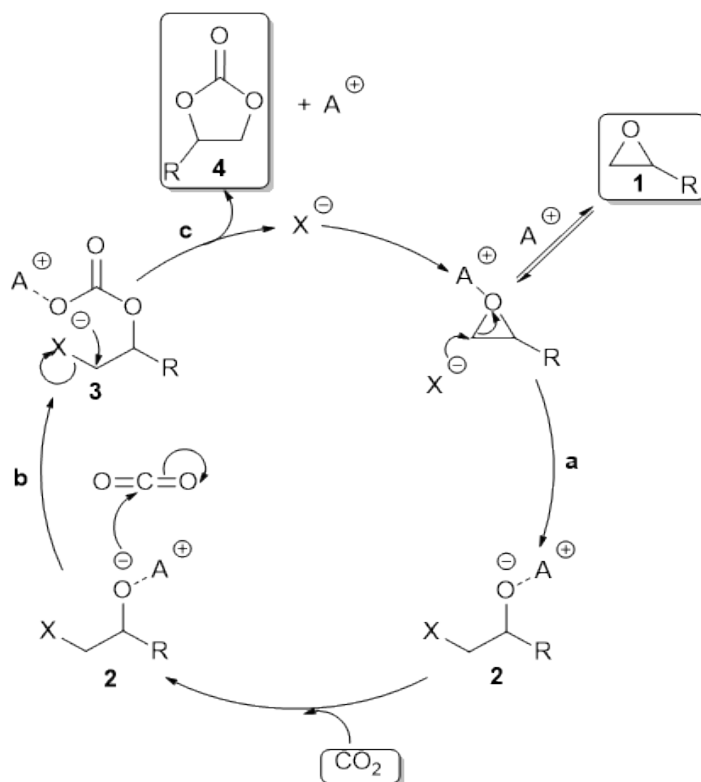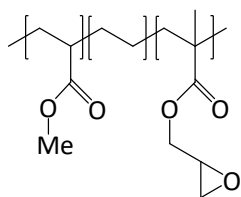

Scheme S1. First route for the cycloaddition of CO_2 with epoxides.
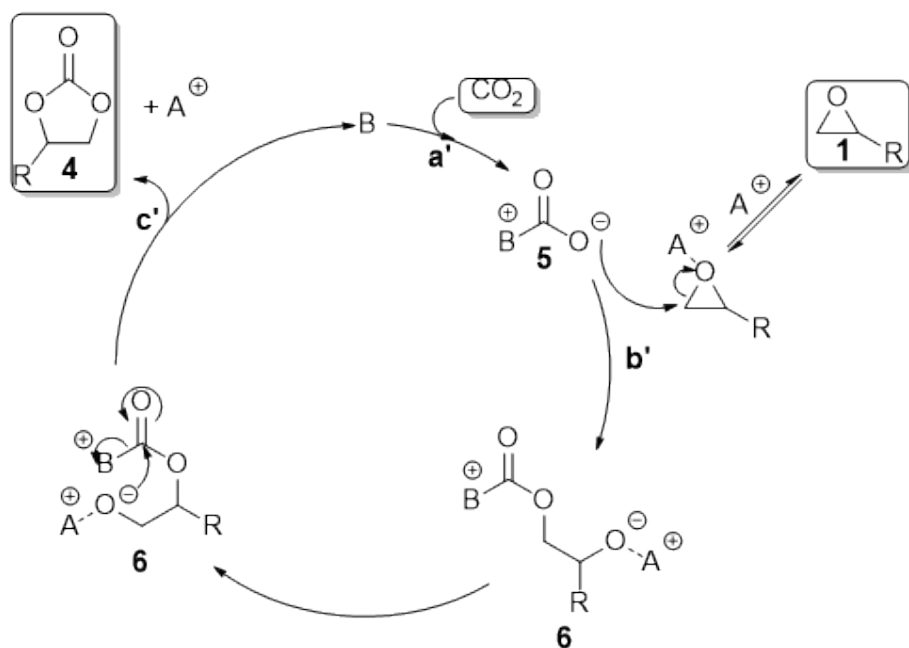
Scheme S2. Second route for the cycloaddition of CO_2 with epoxides.

2. Structure and mains properties of the commercial polymers
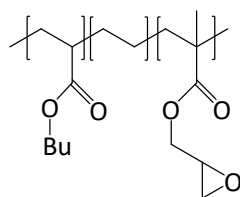

Lotader® AX8900
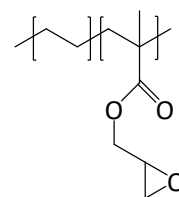methyl acrylate: 24 wt%
glycidyl methacrylate: 8 wt%
$T_f = 65\ °C$

Lotader® AX8700
butyl acrylate: 25 wt%
glycidyl methacrylate: 8 wt%
$T_f = 72\ °C$

Lotader® AX8840
glycidyl methacrylate: 8 wt%
$T_f = 104\ °C$

Scheme S3. Structure and main properties of Lotader® AX8900, AX8700 and AX8840.

3. Characterization of glycidyl methacrylate and the commercial polymers
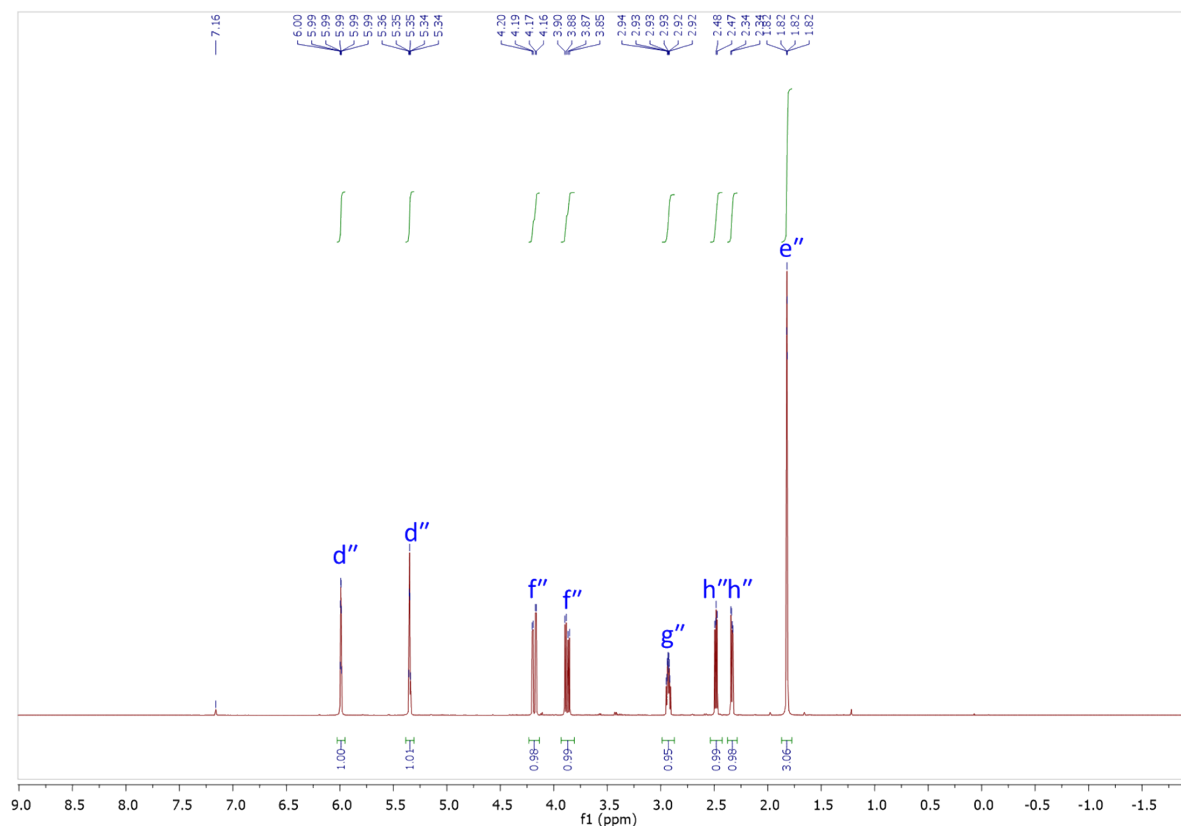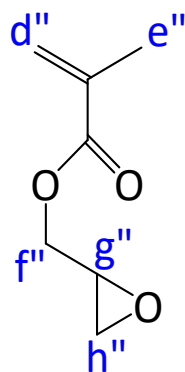
a. ¹H NMR spectra

Figure S1. ¹H NMR (TCE/C$_6$D$_6$, 400 MHz) spectrum of glycidyl methacrylate (GMA).

¹H NMR (400 MHz, TCE/C$_6$D$_6$) δ: 5.99 (m, 1H, d″), 5.35 (m, 1H, d″), 4.18 (dd, J = 12.2, 3.6 Hz, 1H, f″), 3.87 (dd, J = 12.2, 5.6 Hz, 1H, f″), 2.99 – 2.87 (m, 1H, g″), 2.48 (dd, J = 5.3, 4.0 Hz, 1H, h″), 2.33 (dd, J = 5.3, 2.5 Hz, 1H, h″), 1.82 (dd, J = 1.6, 1.0 Hz, 3H, e″).
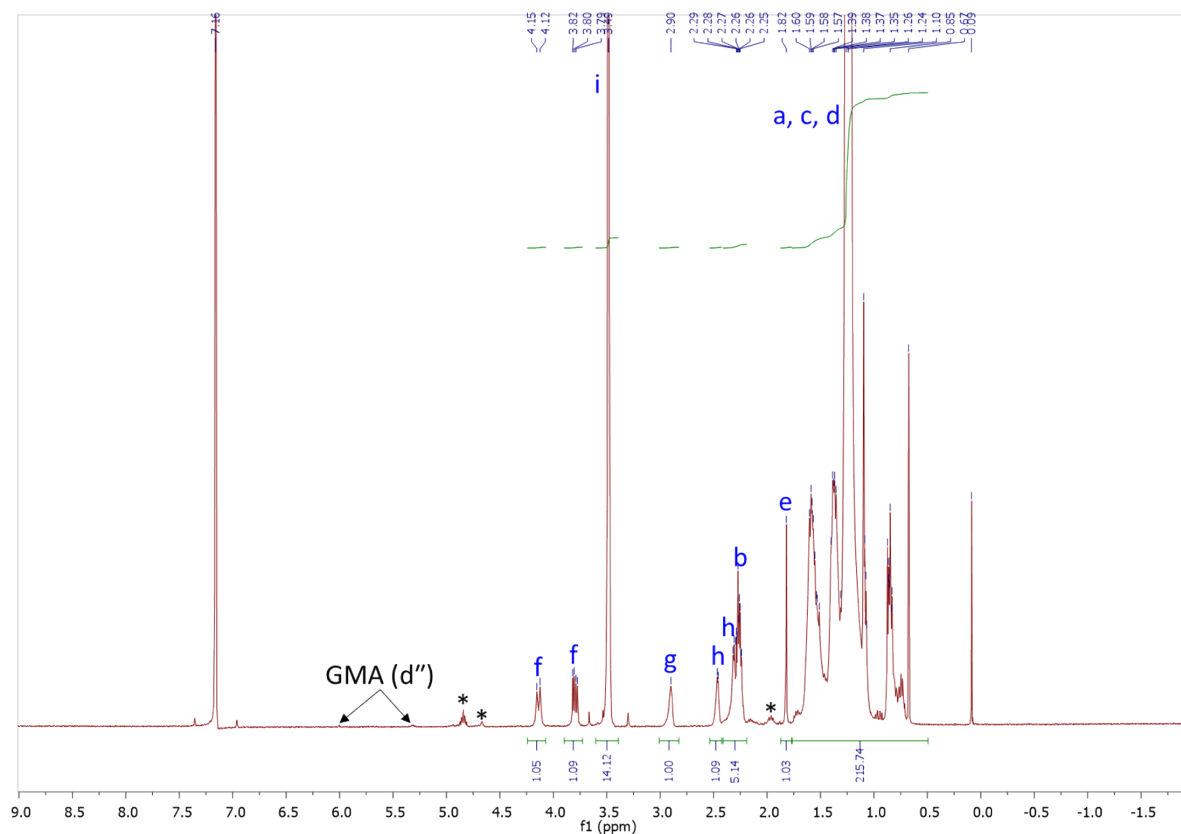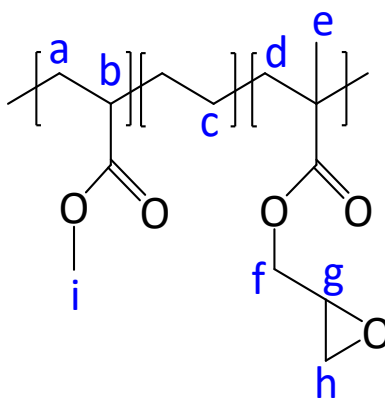
Figure S2. ^{1}H NMR (TCE/C$_6$D$_6$, 400 MHz) spectrum of the Lotader® AX8900.

^{1}H NMR (400 MHz, TCE/C$_6$D$_6$) δ: 4.14 (dd, J = 12.0, 3.7 Hz, f), 3.80 (dd, J = 12.1, 5.6 Hz, f), 3.49 (s, i), 2.90 (m, g), 2.46 (m, h), 2.41 – 2.19 (m, b, h), 1.82 – 0.49 (m, a, c, d, e).

*: chain ends due to the radical copolymerization (termination by disproportionation) method used to synthesize these ethylene-rich copolymers[28] ; almost no residual GMA monomer is present (see minute amounts identified under arrows and correspondence with Figure S1)
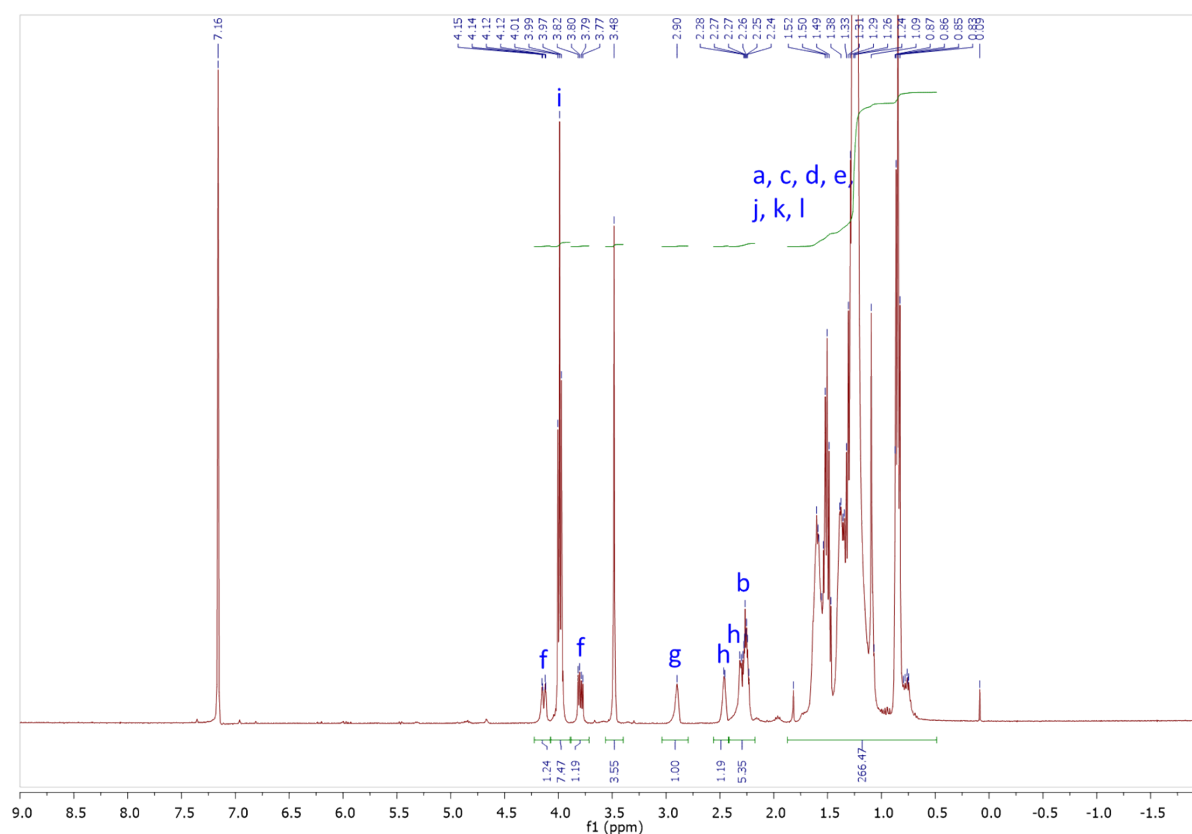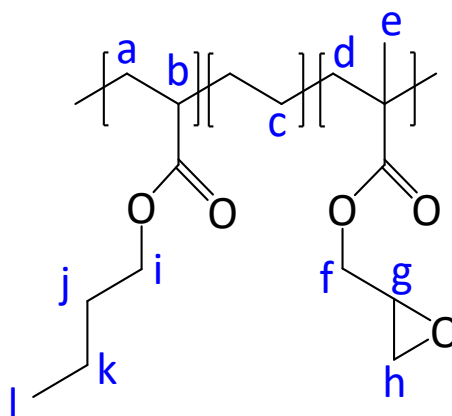
7

Figure S3. ^{1}H NMR (TCE/C$_6$D$_6$, 400 MHz) spectrum of the Lotader® AX8700.

^{1}H NMR (400 MHz, TCE/C$_6$D$_6$) δ : 4.13 (dd, J = 11.4, 2.9 Hz, f), 3.99 (t, J = 6.6 Hz, i), 3.79 (dd, J = 12.1, 5.6 Hz, f), 3.48 (s, 3H, methyl acrylate), 2.90 (m, g), 2.46 (m, h), 2.41 – 2.18 (m, b, h), 1.87 – 0.54 (m, a, c, d, e, j, k, l).
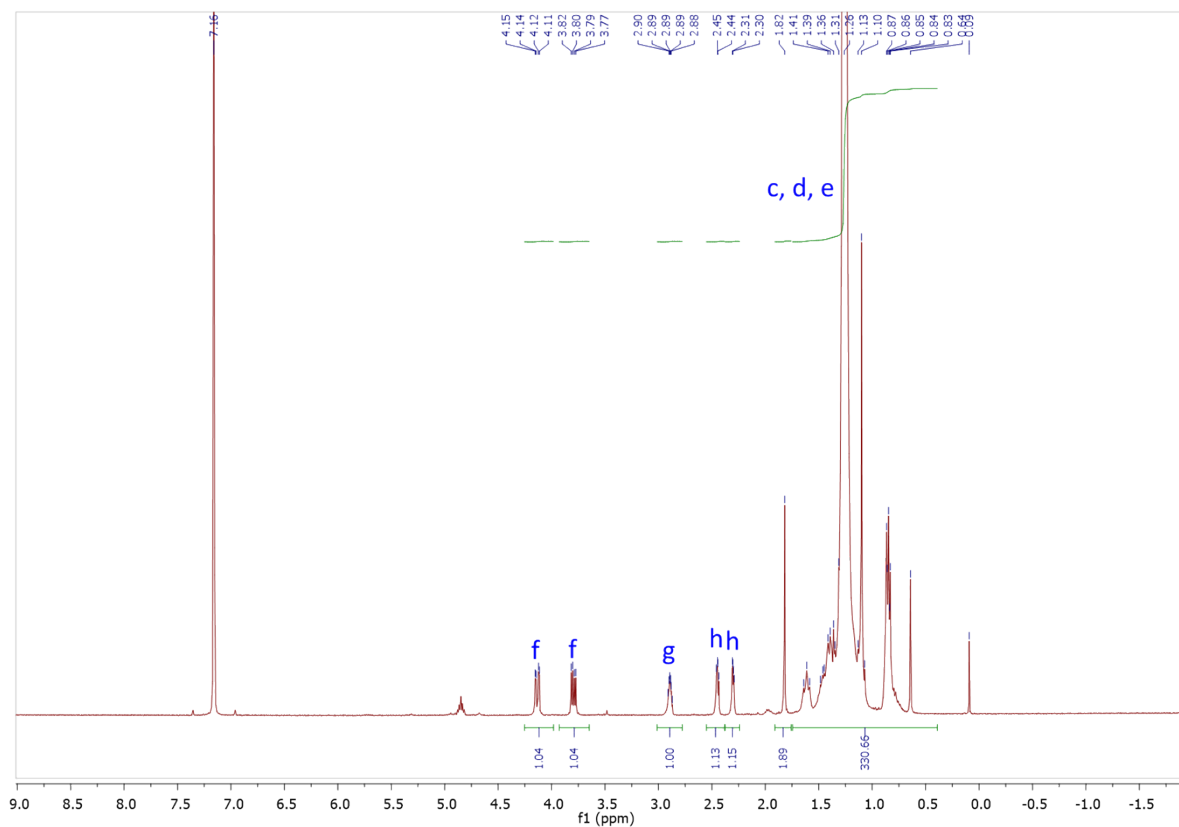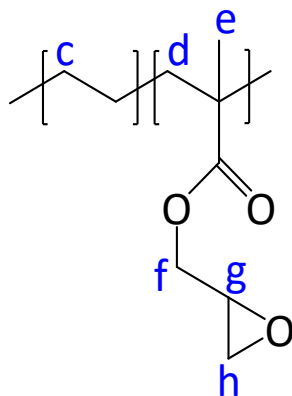
Figure S4. ^{1}H NMR (TCE/C$_6$D$_6$, 400 MHz) spectrum of the Lotader® AX8840.

^{1}H NMR (400 MHz, TCE/C$_6$D$_6$) δ : 4.13 (dd, J = 12.1, 3.7 Hz, f), 3.79 (dd, J = 12.1, 5.6 Hz, f), 3.01 – 2.83 (m, g), 2.45 (dd, J = 5.1, 4.1 Hz, h), 2.30 (dd, J = 5.3, 2.4 Hz, h), 1.87 – 0.37 (m, c, d, e).
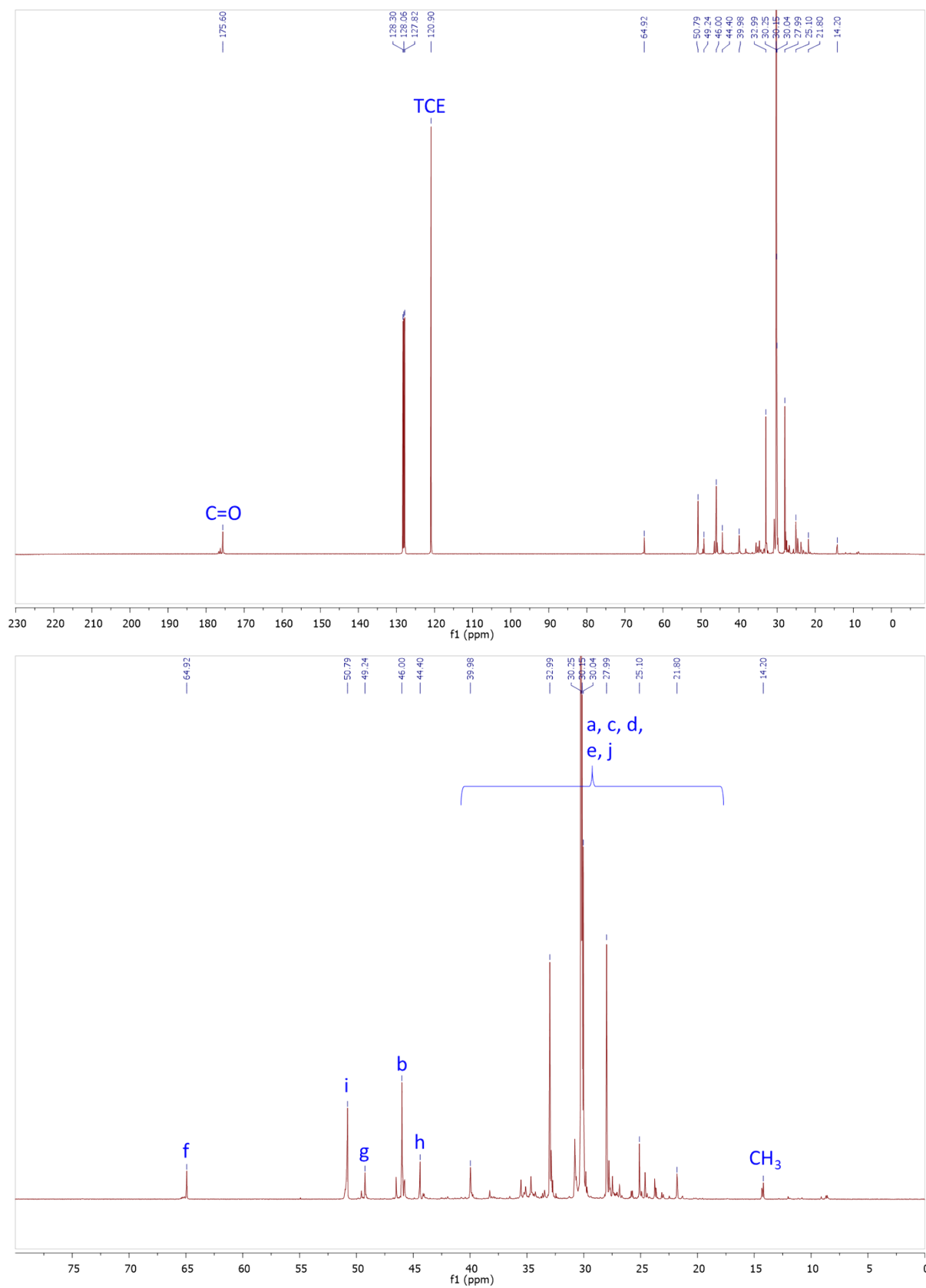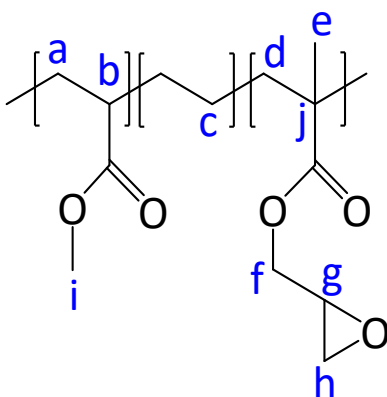
9

b. ^{13}C NMR spectrum

Figure S5. ^{13}C NMR (101 MHz, TCE/C$_6$D$_6$) spectrum of the Lotader® AX8900.

^{13}C NMR (101 MHz, TCE/C$_6$D$_6$) δ: 175.60 (C=O), 64.92 (f), 50.79 (i), 49.24 (g), 46.00 (b), 44,40 (h), 41.27 – 18.04 (a, c, d, e, j), 14.20 (CH$_3$).
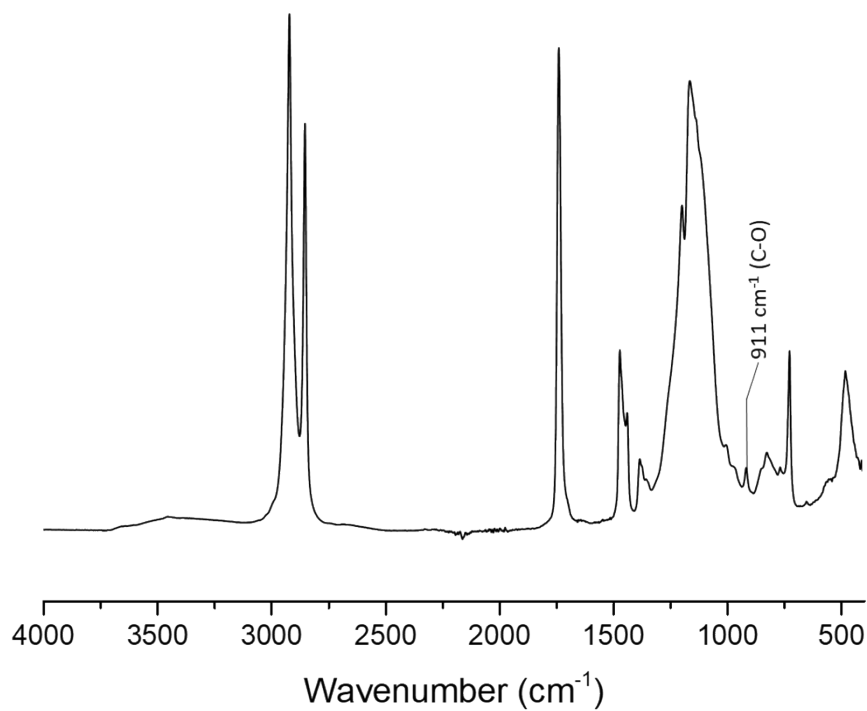
c. <u>ATR-IR spectra</u>
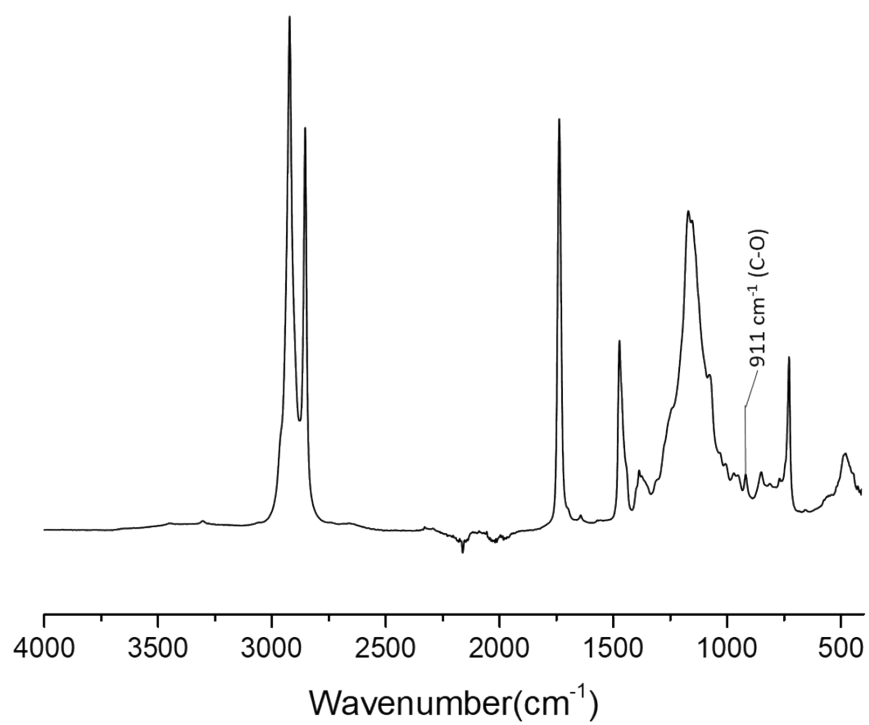

Figure S6. ATR-IR spectrum of Lotader® AX8900.
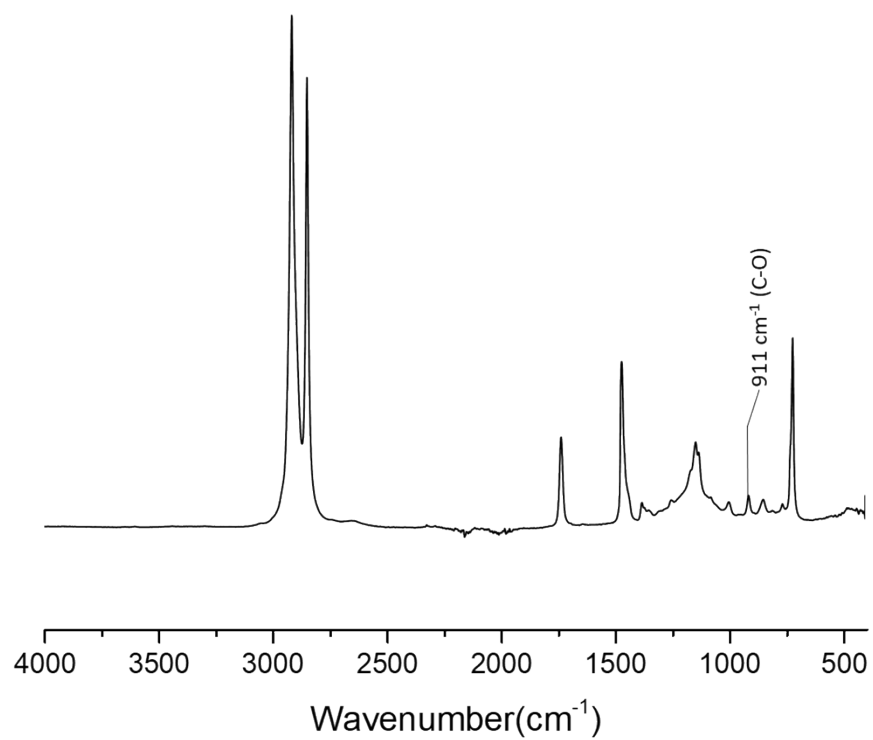
Figure S7. ATR-IR spectrum of Lotader® AX8700.

Figure S8. ATR-IR spectrum of the Lotader® AX8840.

d. <u>SEC analyses</u>
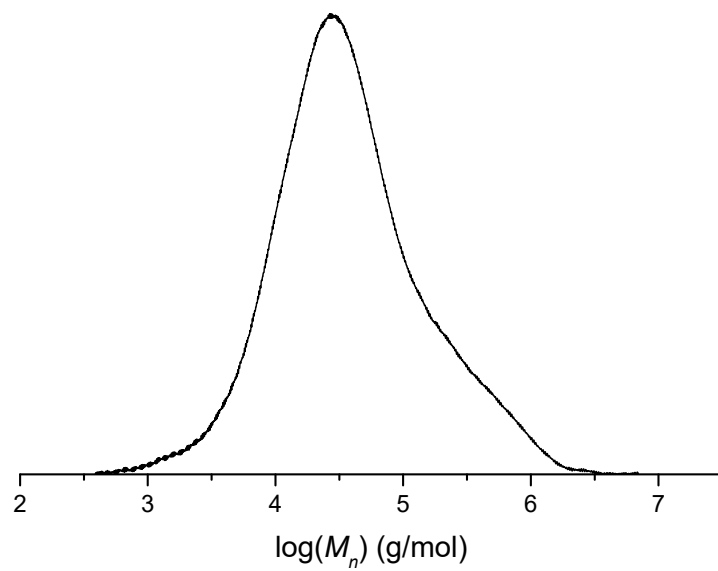
M_n	M_w
16 600	101 300

Figure S9. Molar mass distribution of the Lotader® AX8900.
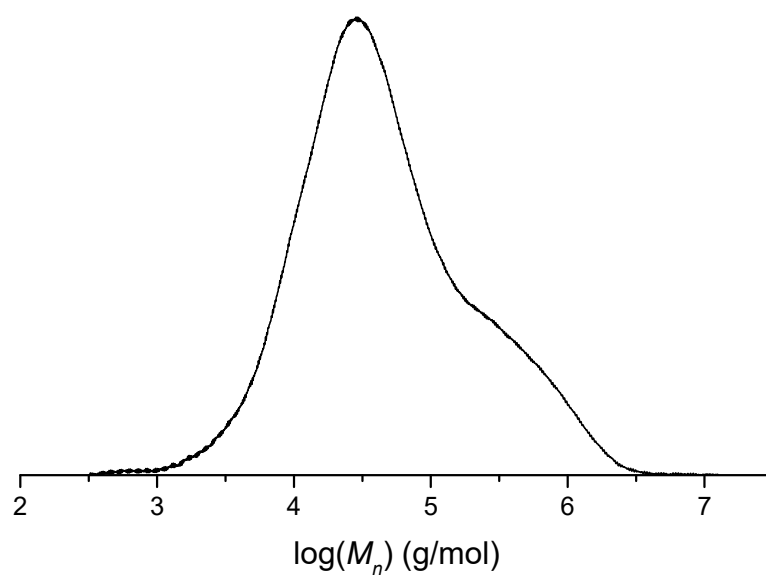
M_n	M_w
18 500	145 000

Figure S10. Molar mass distribution of the Lotader® AX8700.
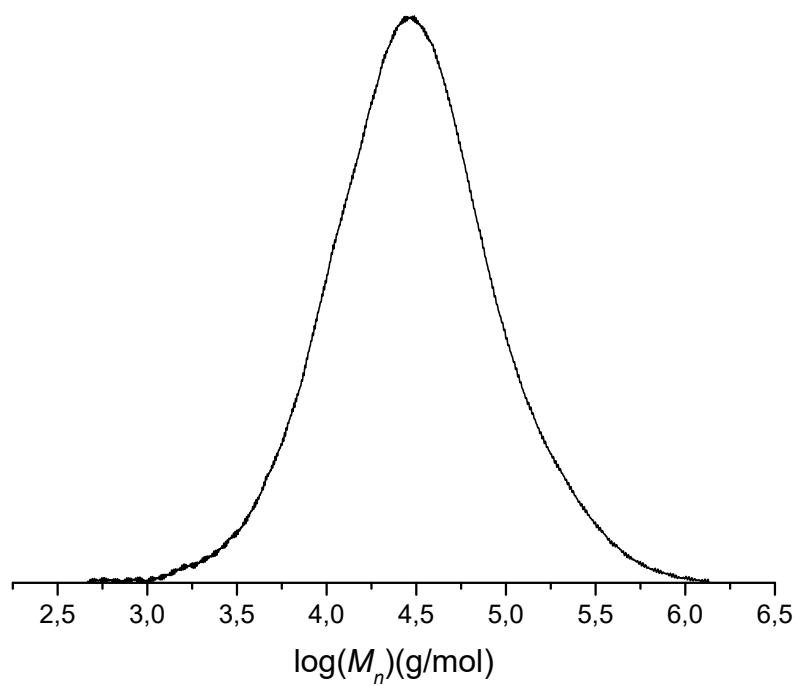
M_n	M_w
17 100	55 500

Figure S11. Molar mass distribution of the Lotader® AX8840.

e. DSC analyses

On the following DSC curves, the glass transition and the melting endotherm of the polymers overlap. Thus, the baseline for the integration of the melting endothermic event is a tangential right line to take into account the change of baseline induced by the glass transition (common practice for DSC of polymers with overlapping thermal events).
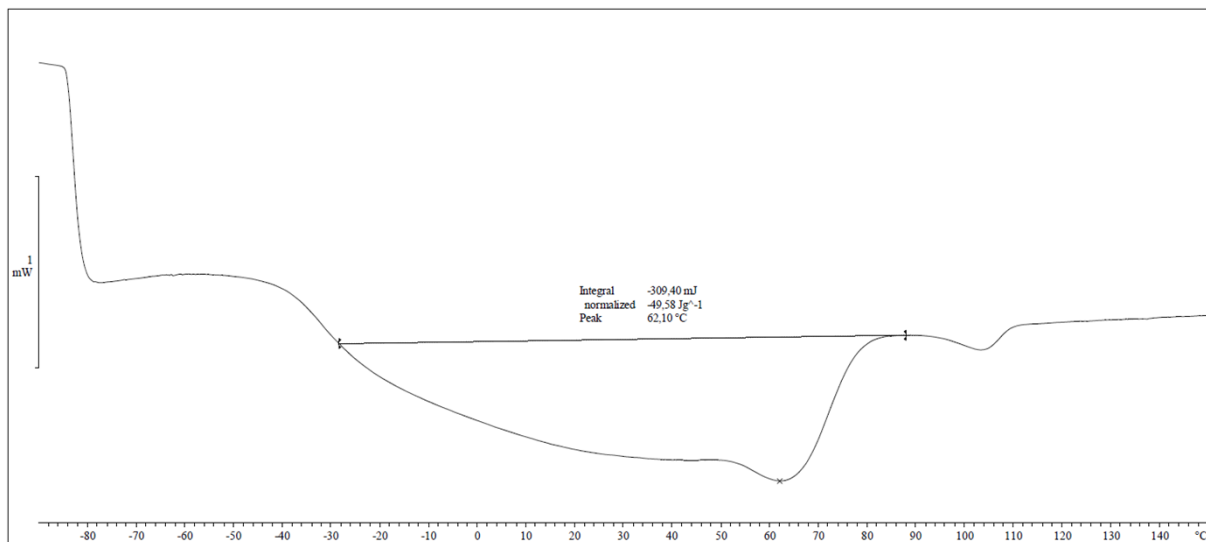

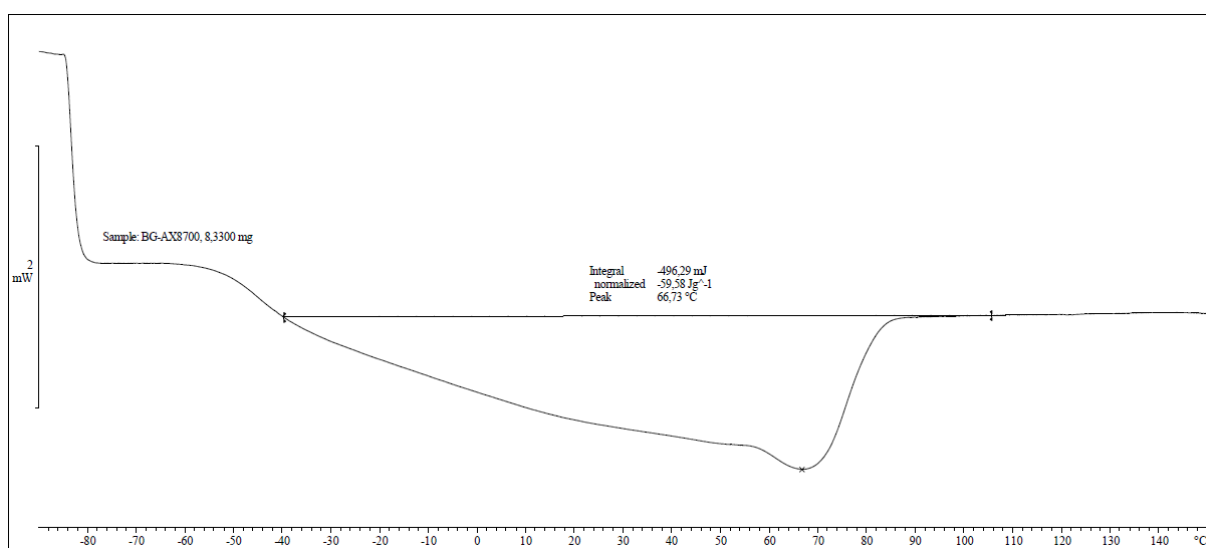**Figure S12.** DSC analysis of the Lotader® AX8900.
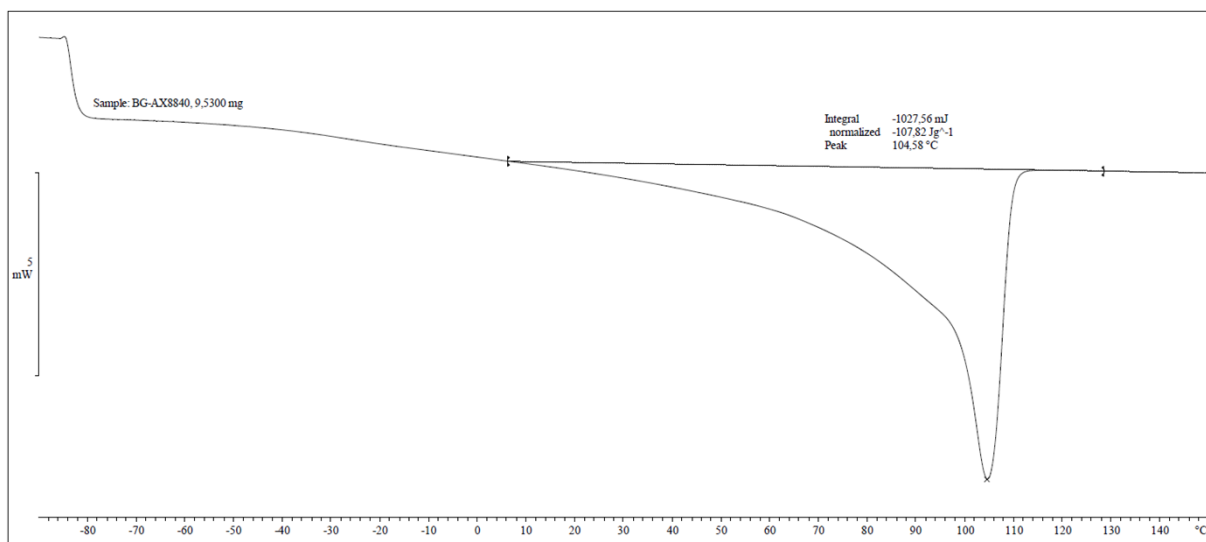

Figure S13. DSC analysis of the Lotader® AX8700.

Sample: BG-AX8840, 9,5300 mg

Integral   -1027,56 mJ
  normalized   -107,82 Jg^-1
Peak   104,58 °C

5 mW

-80 -70 -60 -50 -40 -30 -20 -10 0 10 20 30 40 50 60 70 80 90 100 110 120 130 140 °C

Figure S14. DSC analysis of the Lotader® AX8840.

f. TGA

$BG-AX8900
BG-AX8900, 9,8000 mg

Step   -98,7959 %
                -9,6820 mg
Residue   1,1633 %
                0,1140 mg
Left Limit   214,43 °C
Right Limit   550,41 °C
Heating Rate   10,00 °Cmin^-1
Type horizontal
Delta Ordinate 9,6820 mg

5 mg

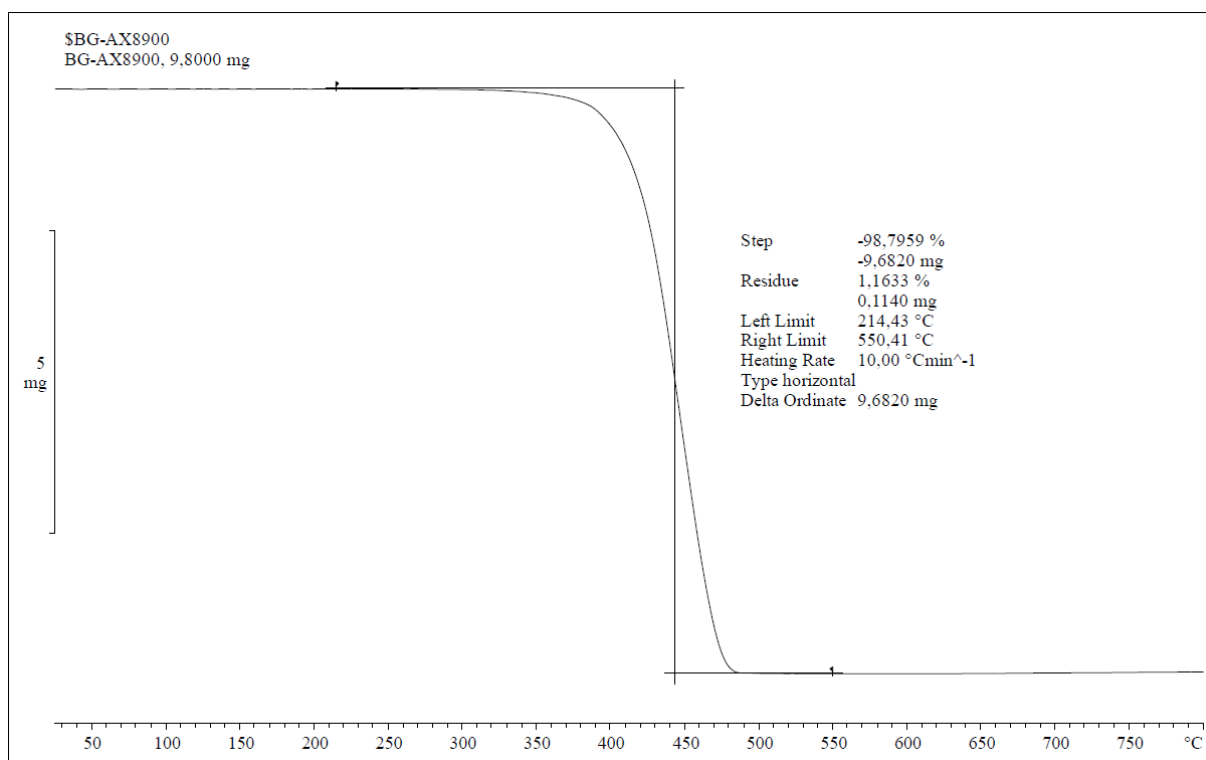50 100 150 200 250 300 350 400 450 500 550 600 650 700 750 °C

Figure S15. TGA analysis of the Lotader® AX8900.

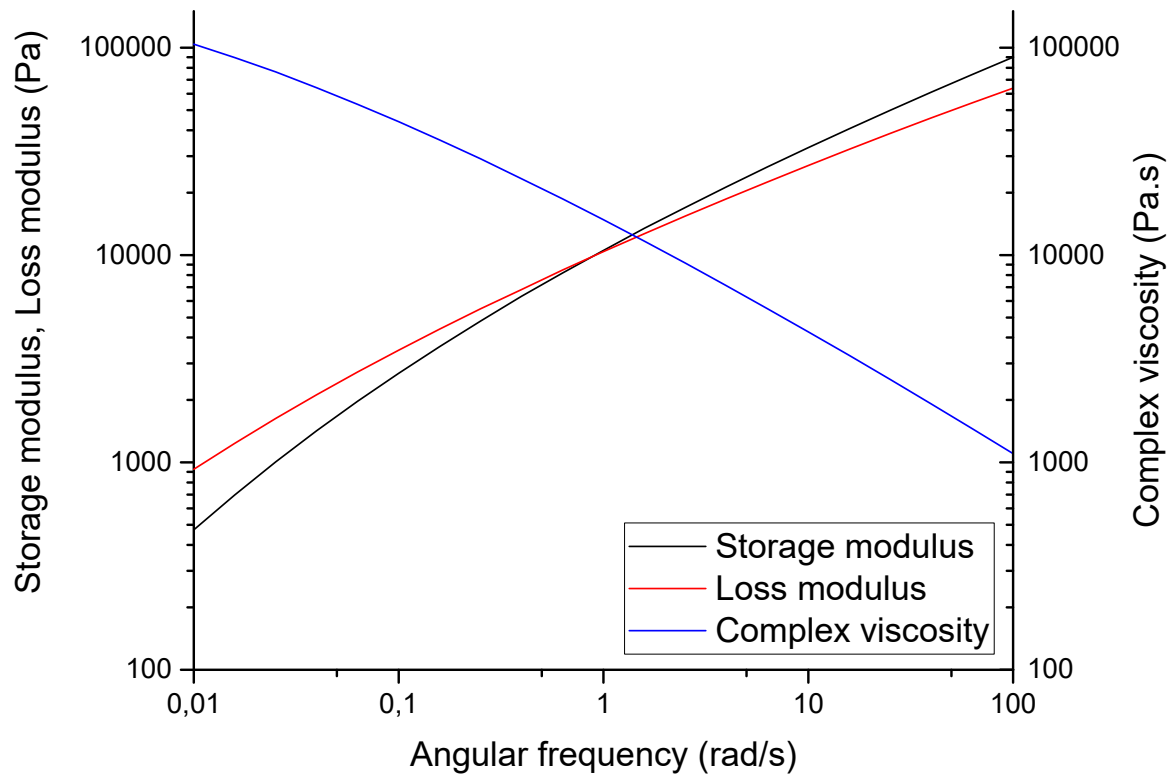g. <u>Rheology analysis</u>

Figure S16. Rheology analysis at 150 °C of the Lotader® AX8900.

4. Establishment of the calibration curve to determine the cyclic carbonate yield

The reaction with TBAB using the Lotader® AX8900 described in **Figure 3** was followed by ^{1}H NMR and ATR-IR (**Figure S17**). The cyclic carbonate yield determined by ^{1}H NMR was correlate to the ratio C=O cyclic carbonate band area (1820 cm^{-1}) / C=O ester band area (1734 cm^{-1}) calculated by ATR-IR. As shown in **Table S1**, for each reaction time, three samples were analyzed by ATR-IR to confirm the homogeneity of the modified polymer, allowing the calculation of an average ratio based on these three different analyses. The linear correlation between the cyclic carbonate yield and the average ratio is shown on **Figure S18**. All the cyclic carbonate yields for the modification of the Lotader® AX8900 were determined using this calibration curve.
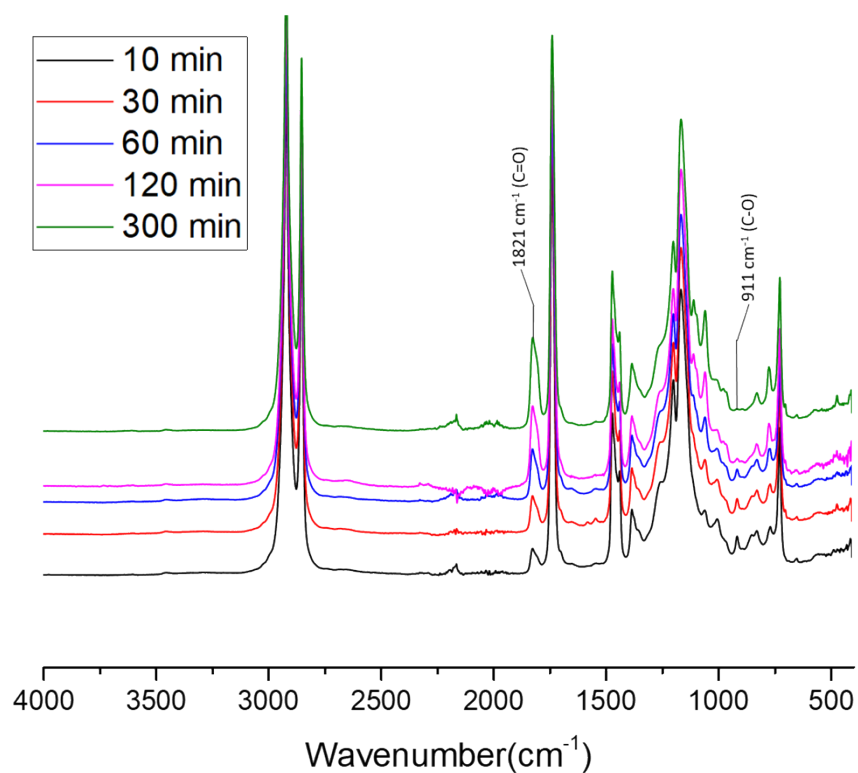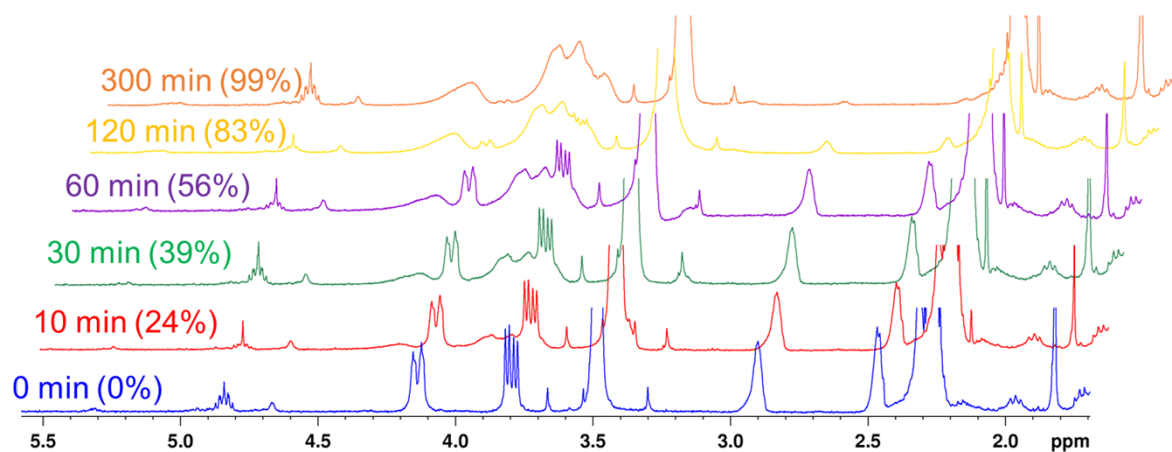
Figure S17. Reaction with TBAB in batch followed by ^{1}H NMR (TCE/C_6D_6, 400MHz) and ATR-IR. [a]Conditions: 2.0 g of Lotader® AX8900 (1.1 mmol of glycidyl methacrylate), 18 mg of TBAB (0.057 mmol, 5 mol%), 2.0 mL of toluene, 110 °C, 4.0 MPa of CO_2.

Table S1. Calculation of the ratio cyclic carbonate C=O band area (1820 cm^{-1}) / ester C=O band area (1734 cm^{-1}) for the reaction with the Lotader® AX8900 using TBAB as catalyst

Reaction time (min)	Cyclic carbonate C=O area	Ester C=O area	Ratio cyclic carbonate C=O area /ester C=O area	Ratio average	Yield (%)
10	0.433	6.200	0.0698		
	0.427	6.053	0.0705	**0.0702**	**24**
	0.428	6.084	0.0703		
30	0.680	6.138	0.1108		
	0.720	5.933	0.1213	**0.1172**	**39**
	0.733	6.140	0.1194		
60	0.999	5.991	0.1668		
	1.074	6.343	0.1693	**0.1638**	**56**
	0.908	5.848	0.1553		
120	1.727	6.423	0.2689		
	1.742	6.406	0.2719	**0.2682**	**83**
	1.647	6.241	0.2639		
300	2.059	6.174	0.3335		
	2.013	6.025	0.3341	**0.3359**	**99**
	2.089	6.145	0.3400		

[a]Conditions: 2.0 g of Lotader® AX8900 (1.1 mmol of glycidyl methacrylate), 18 mg of TBAB (0.057 mmol, 5 mol%), 2.0 mL of toluene, 110 °C, 4.0 MPa of CO_2.
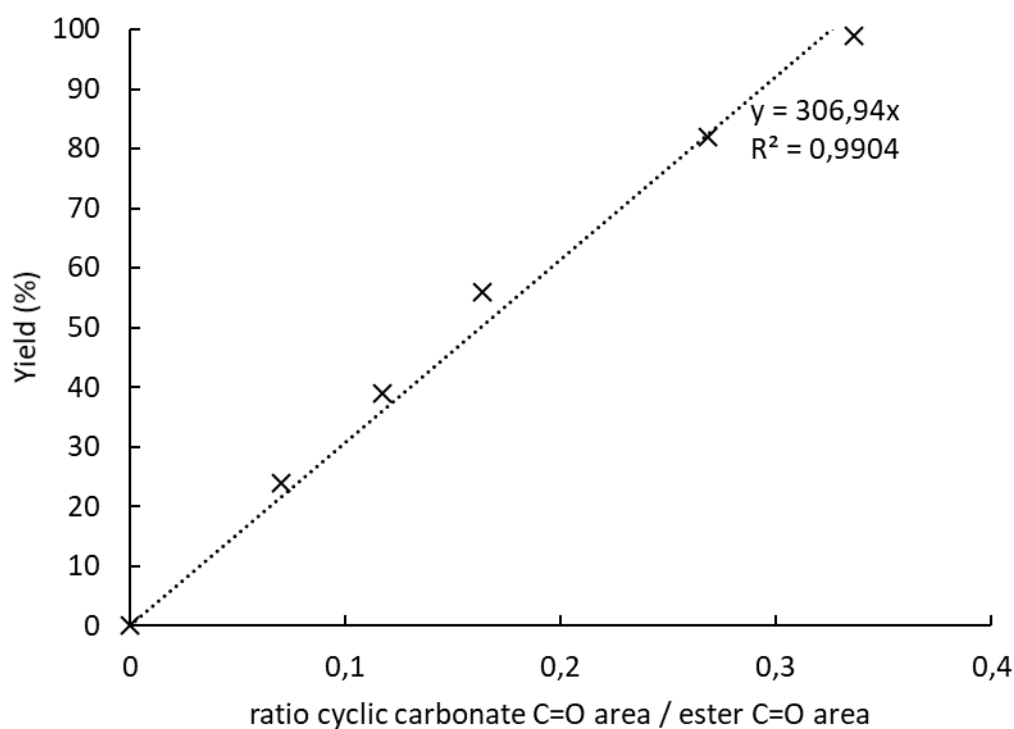

Figure S18. Calibration curve for the calculation of the cyclic carbonate yield with Lotader® AX8900 established from **Table S1**.
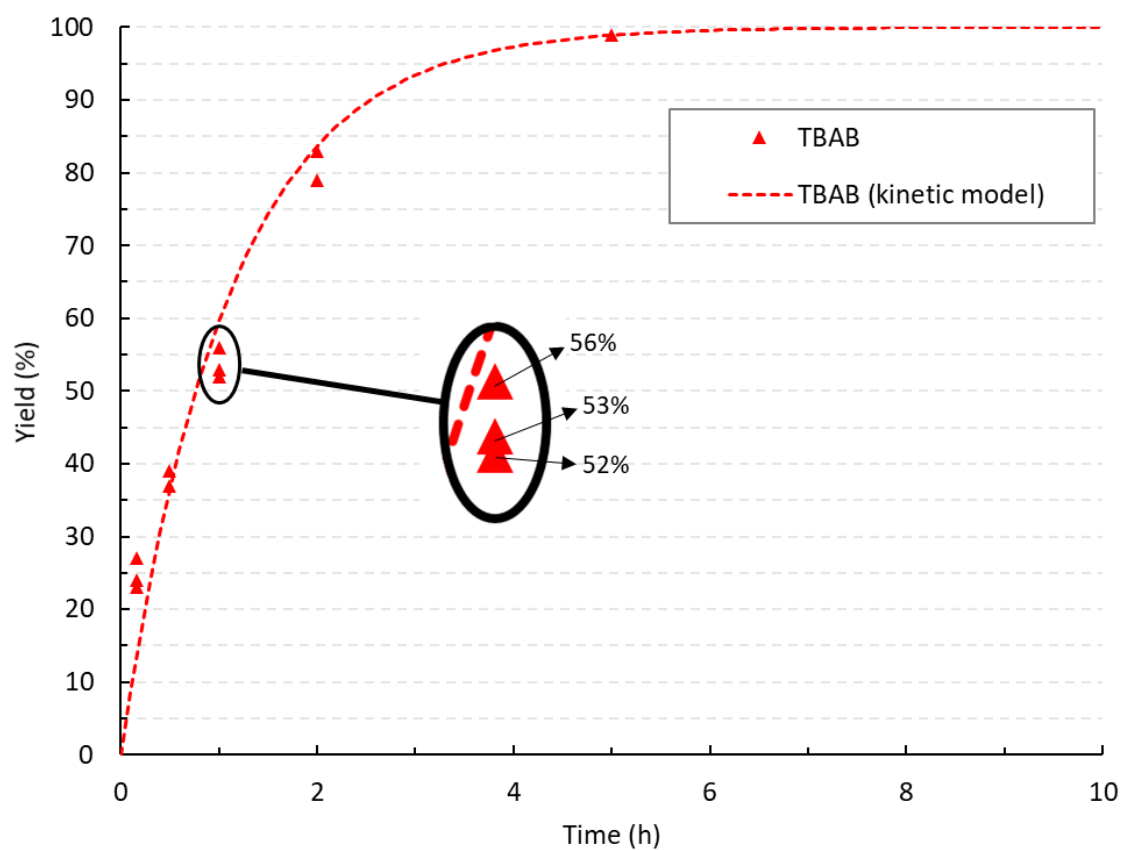
5. Repeatability of the experiments

Figure S19. Repeated experiments for the reactions with TBAB

6. Characterization of the modified polymers with CO_2 in batch
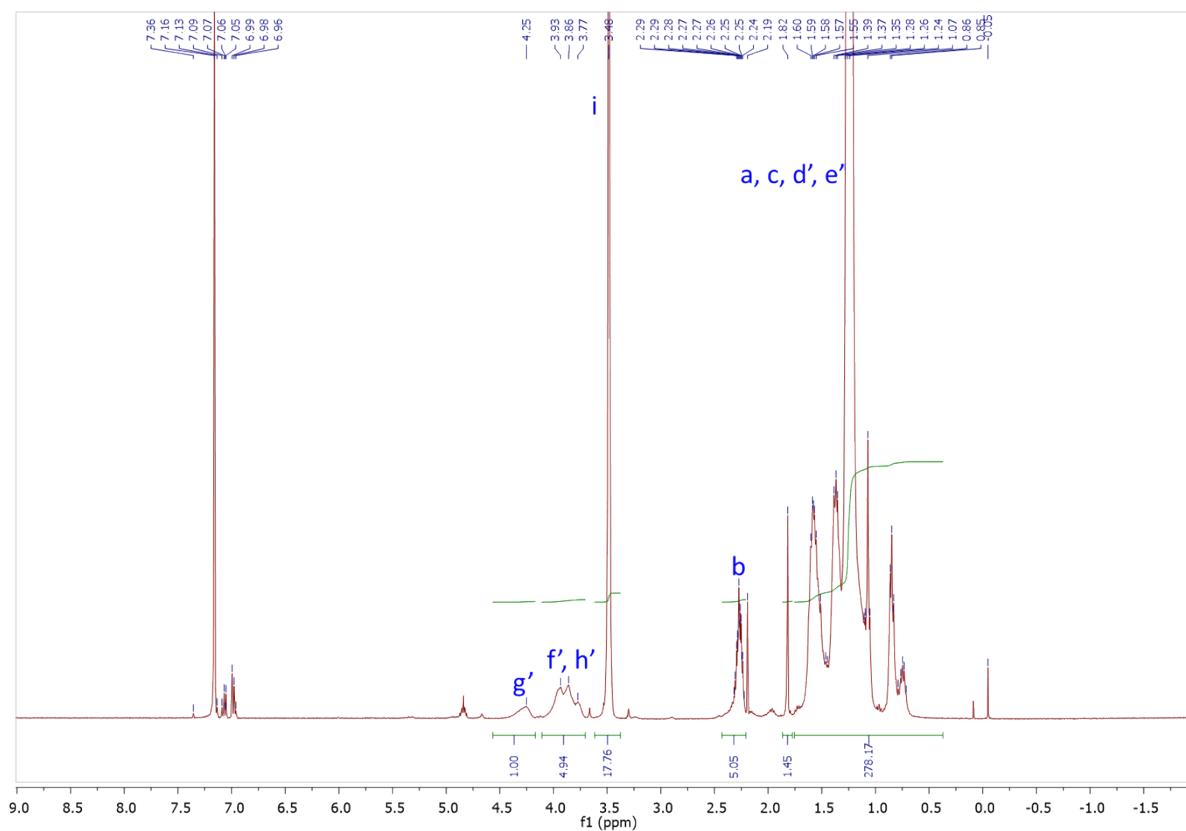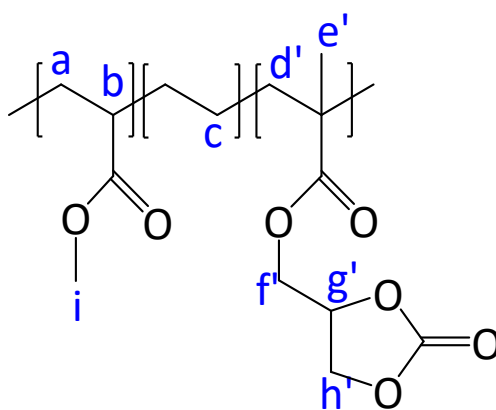
a. <u>^{1}H NMR spectra</u>

Figure S20. ^{1}H NMR (TCE/C$_6$D$_6$, 400 MHz) spectrum of the modified Lotader® AX8900 with CO_2 in batch.

^{1}H NMR (400 MHz, TCE/C$_6$D$_6$) δ: 4.25 (m, g'), 4.07 – 3.70 (m, f', h'), 3.48 (s, i), 2.38 – 2.21 (m, b), 1.84 – 0.33 (m, a, c', d', e').
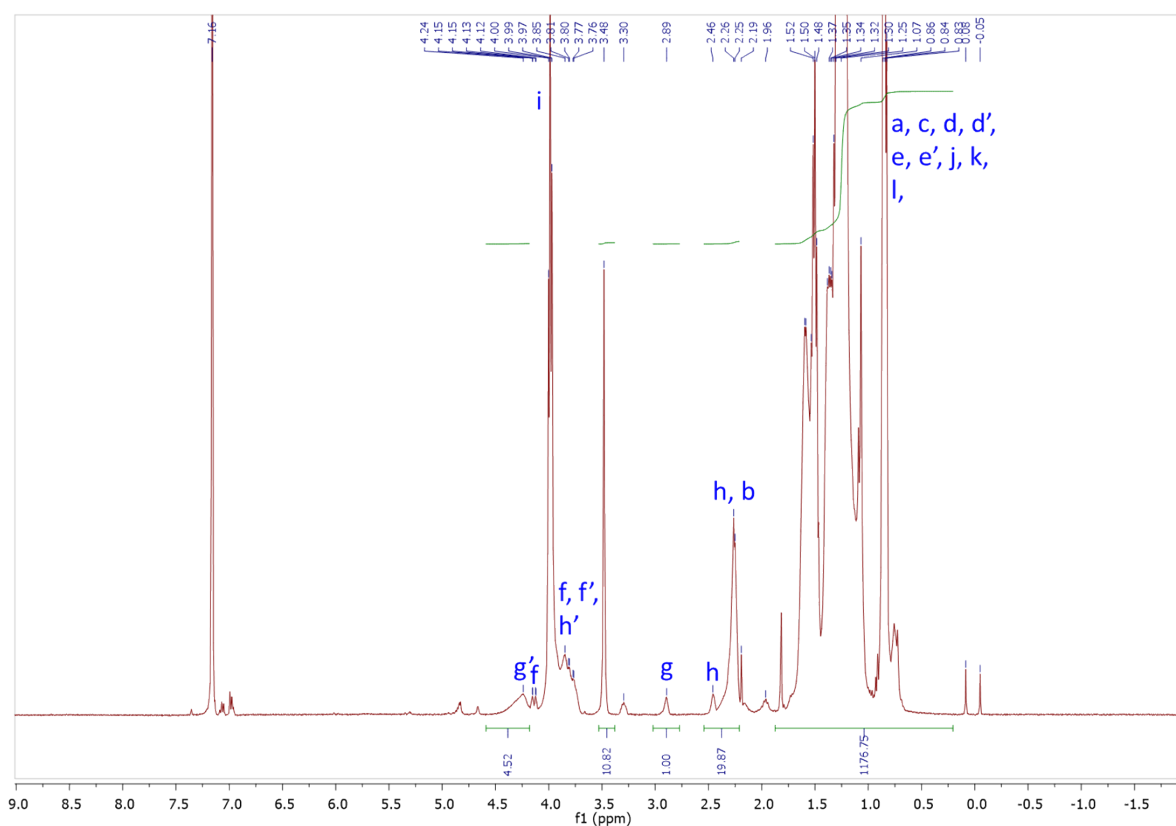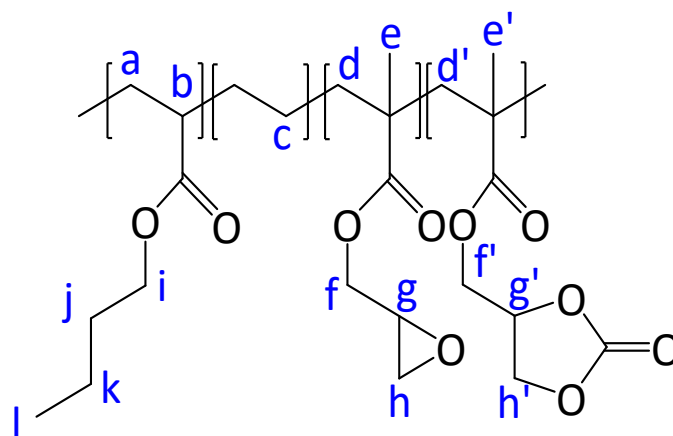
Figure S21. ^{1}H NMR (TCE/C$_6$D$_6$, 400 MHz) spectrum of the modified Lotader® AX8700 with CO$_2$ in batch.

^{1}H NMR (400 MHz, TCE/C$_6$D$_6$) δ: 4.24 (m, g'), 4.14 (dd, J = 11.4, 2.9 Hz, f), 4.09 – 3.69 (m, f, f', h', i), 3,48 (methyl acrylate), 2.89 (m, g), 2.53 – 2.21 (m, h, b), 1.88 – 0.37 (m, a, c, d, d', e, e', j, k, l).

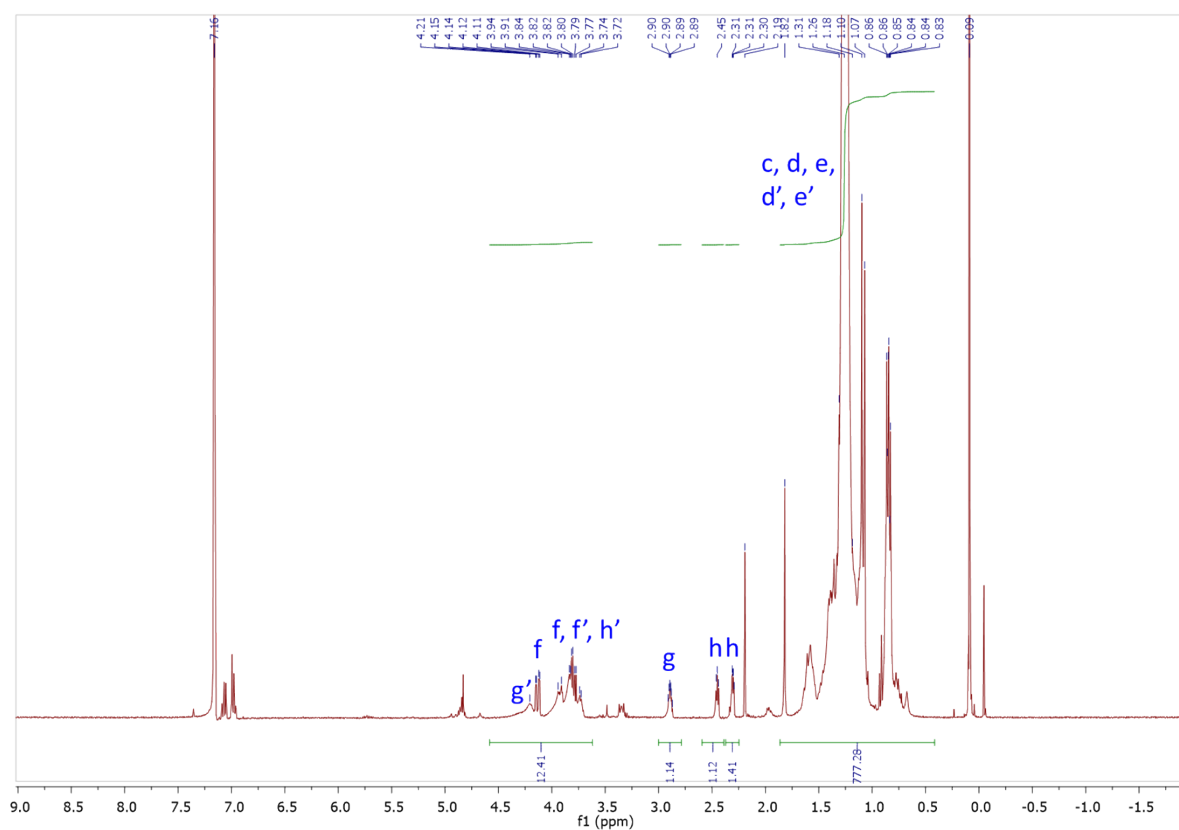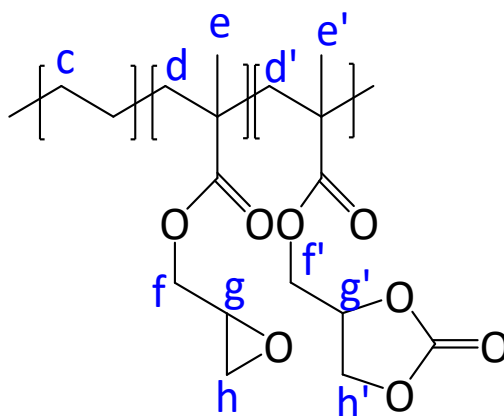$$Yield\ of\ cyclic\ carbonate = \frac{S_{g'}}{S_g + S_{g'}} = \frac{4.52}{4.52 + 1.00} = 82\ \%$$

Figure S22. ^{1}H NMR (TCE/C$_6$D$_6$, 400 MHz) spectrum of the Lotader® AX8840 modified with CO$_2$ in batch.

^{1}H NMR (400 MHz, TCE/C$_6$D$_6$) δ : 4.51 – 3.66 (m, g', f, f', h'), 2.90 (m, g), 2.45 (dd, J = 5.1, 4.1 Hz, h), 2.30 (dd, J = 5.3, 2.4 Hz, h), 1.87 – 0.45 (m, c, d, d', e, e').

$$\textit{Yield of cyclic carbonate } = \frac{S_{f'} + S_{g'} + S_{h'}}{S_f + S_g + S_h + S_{f'} + S_{g'} + S_{h'}} = \frac{11.95 - 1.17 \times 2}{1.00 + 1.10 + 1.40 + 11.95} = 62\%$$
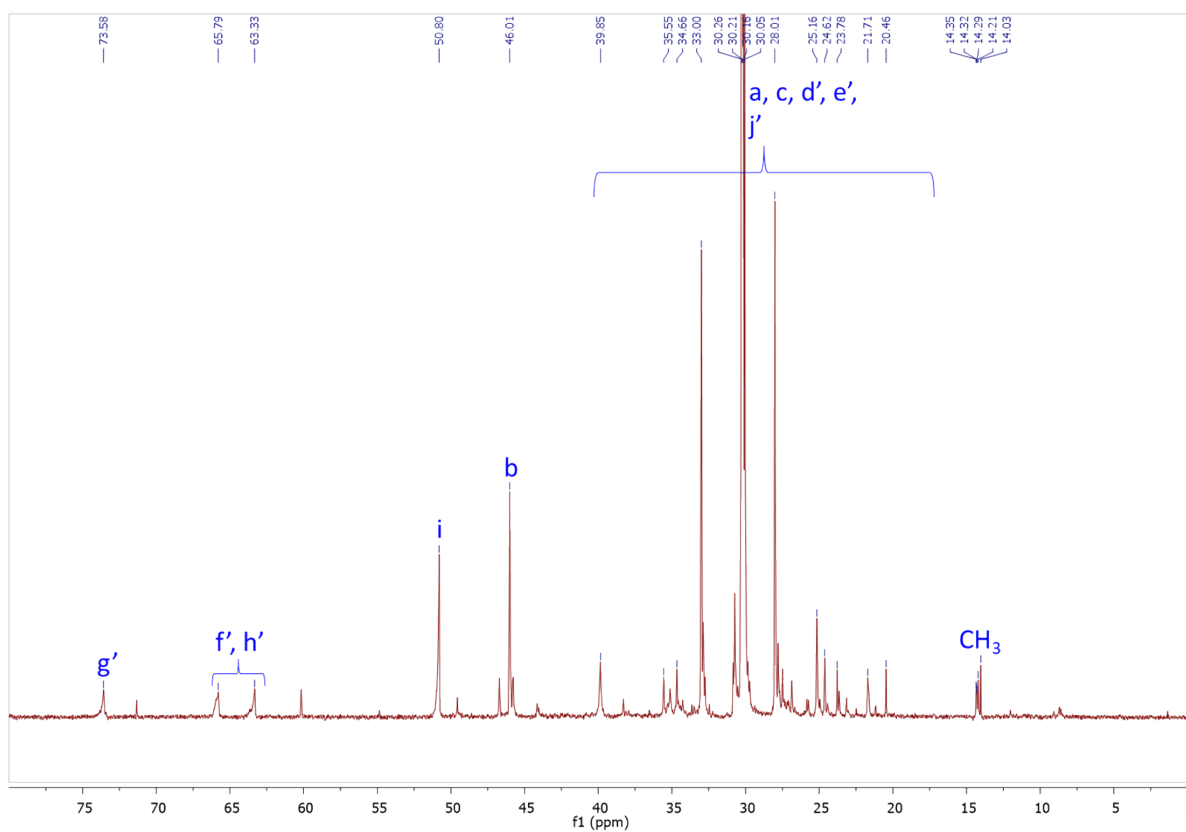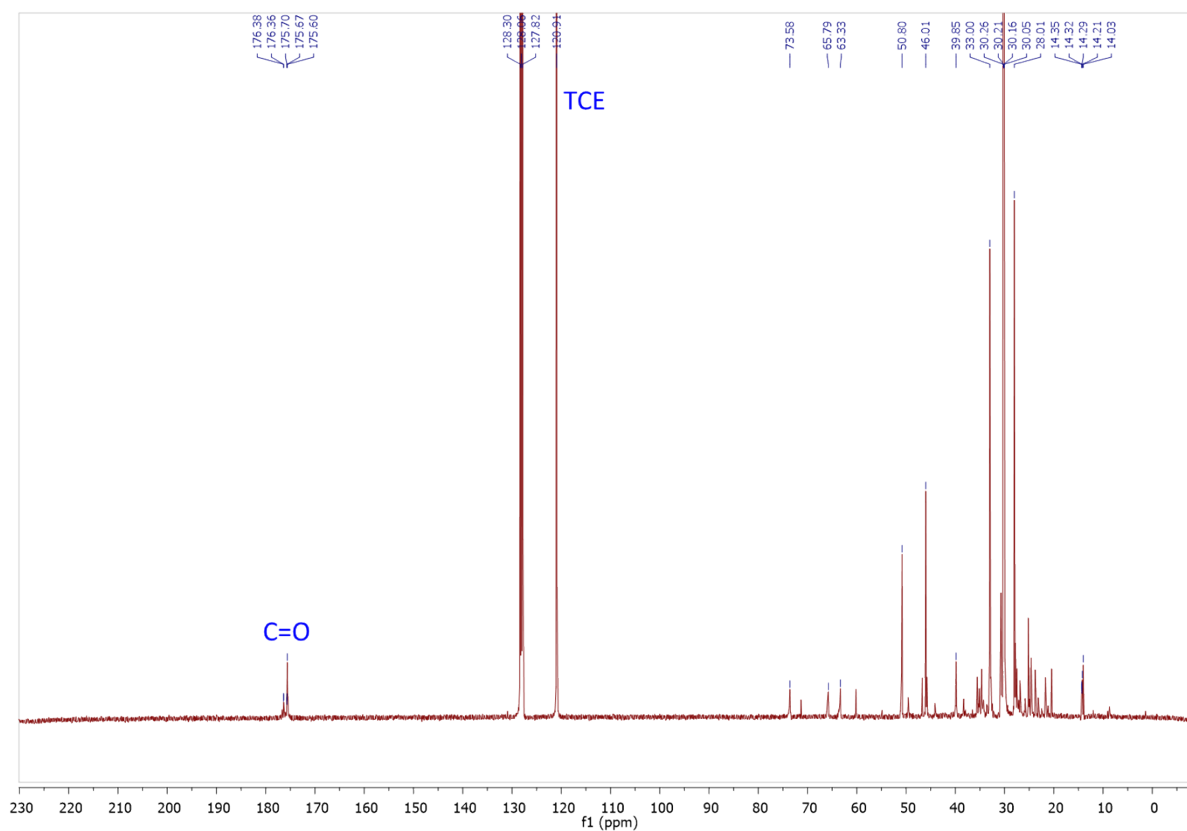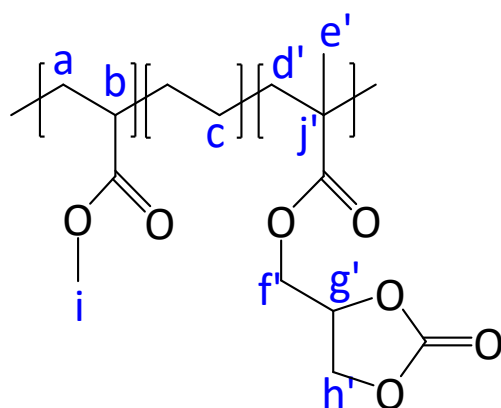
b. <u>^{13}C NMR spectrum</u>

Figure S23. ^{13}C NMR (101 MHz, TCE/C$_6$D$_6$) spectrum of the Lotader® AX8900 modified with CO$_2$ in batch.

^{13}C NMR (101 MHz, TCE/C$_6$D$_6$) δ: 175.60 (C=O), 120.91 (TCE), 73.58 (g'), 65.79 – 63.33 (f', h'), 50.80 (i), 46.01 (b), 39.85 – 20.46 (a, c, d', e', j'), 14.35-14.03 (CH$_3$).
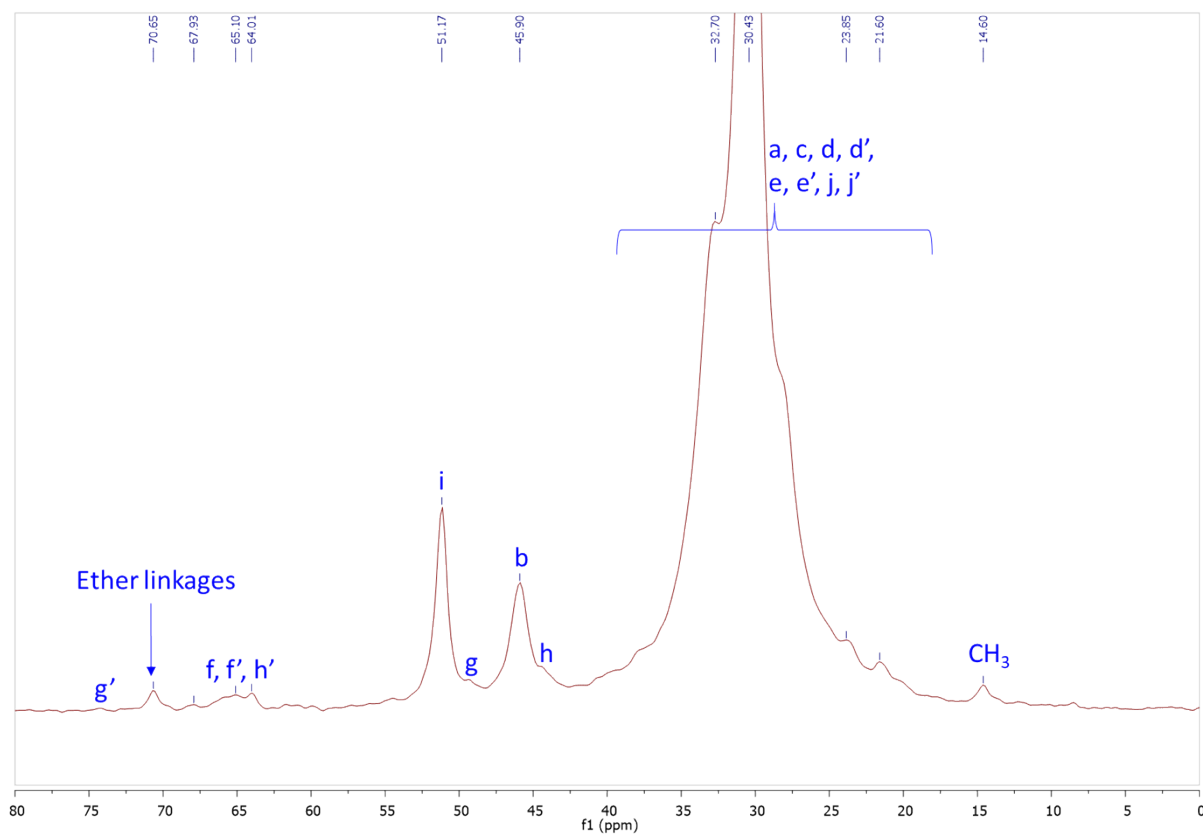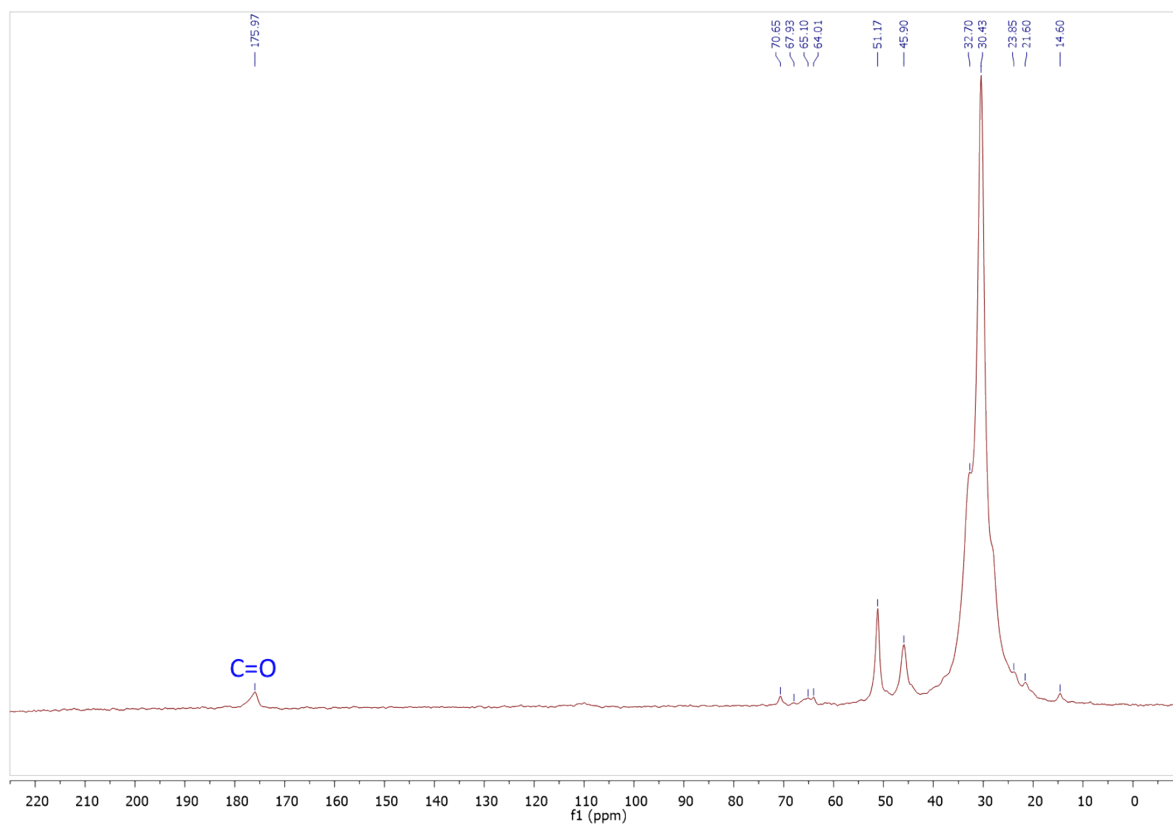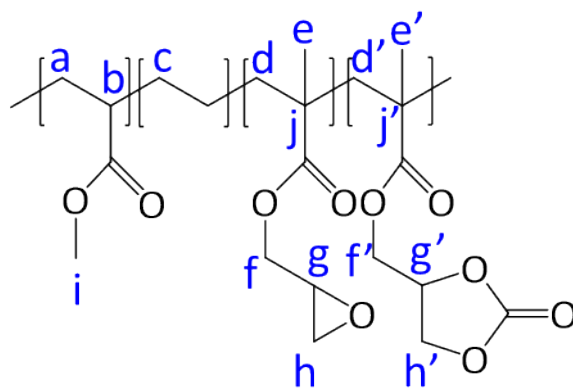
Figure S24. CP/MAS ^{13}C NMR (126 MHz) spectrum of the Lotader® AX8900 modified with CO_2 and catalyzed by TBAC in batch.

CP/MAS ^{13}C NMR (126 MHz) δ 175.97 (C=O), 74.25 (g'), 70.65 (ether linkages), 69.19 – 62.61 (f, f', h'), 51.17 (i), 49.38 (g), 45.90 (b), 41.59 – 18.59 (a, c, d, d', e, e', j, j'), 14.60 (CH$_3$).
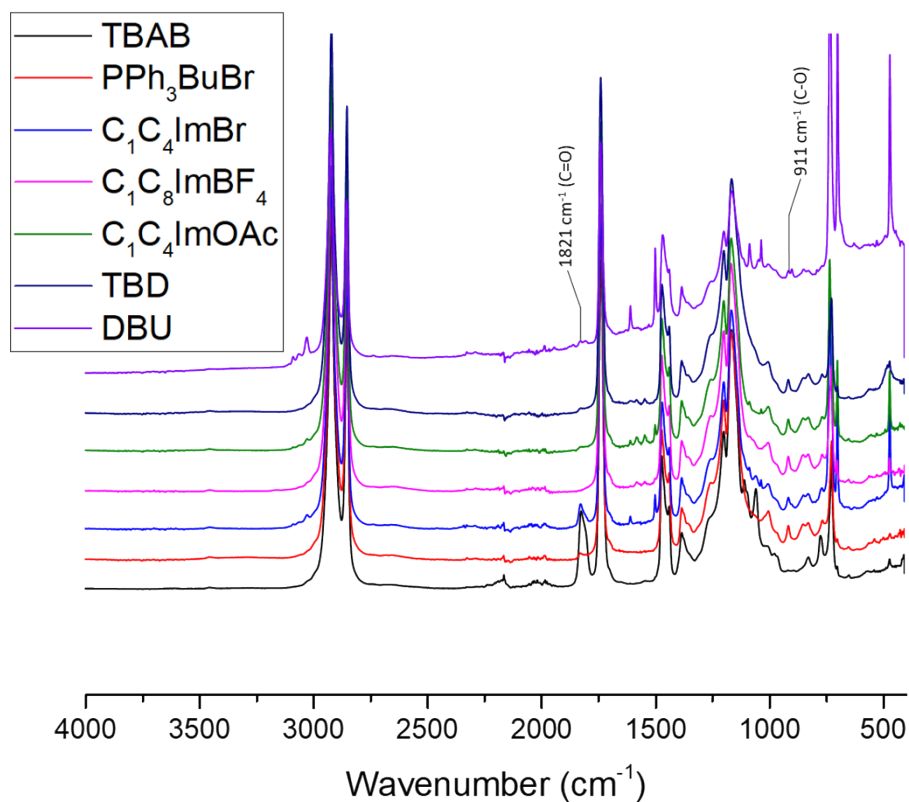
c. ATR-IR spectra

Figure S25. ATR-IR spectra of the Lotader® AX8900 modified with CO_2 (catalyst (5 mol%), 110°C, 4 MPa, toluene, 5 h) using different catalysts in batch.
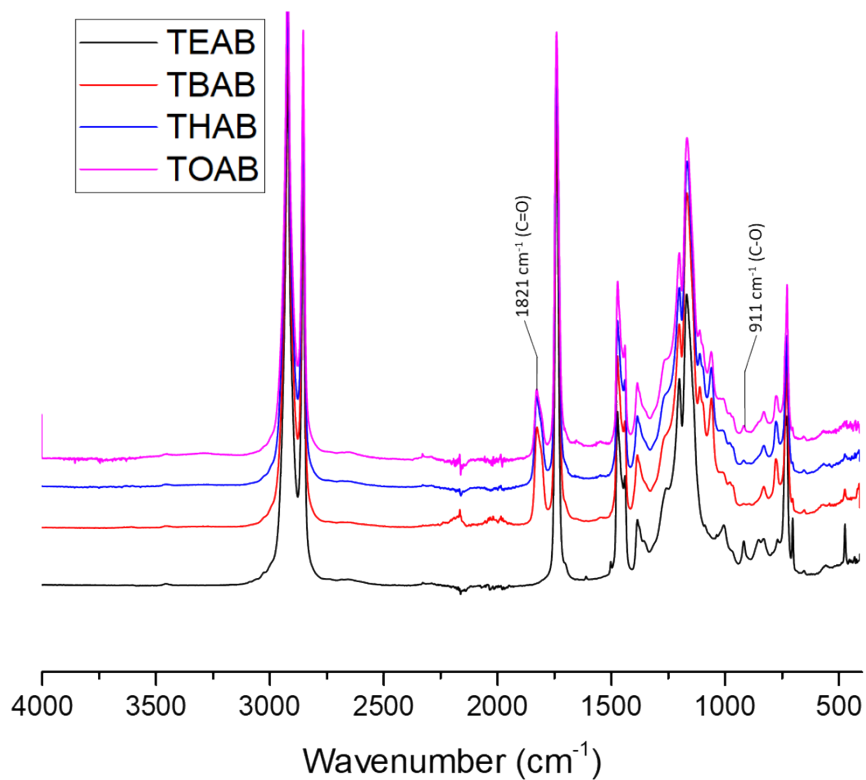
Figure S26. ATR-IR spectra of the Lotader® AX8900 modified with CO_2 (catalyst (5 mol%), 110°C, 4 MPa, toluene, 5 h) using different alkylammonium bromides in batch.
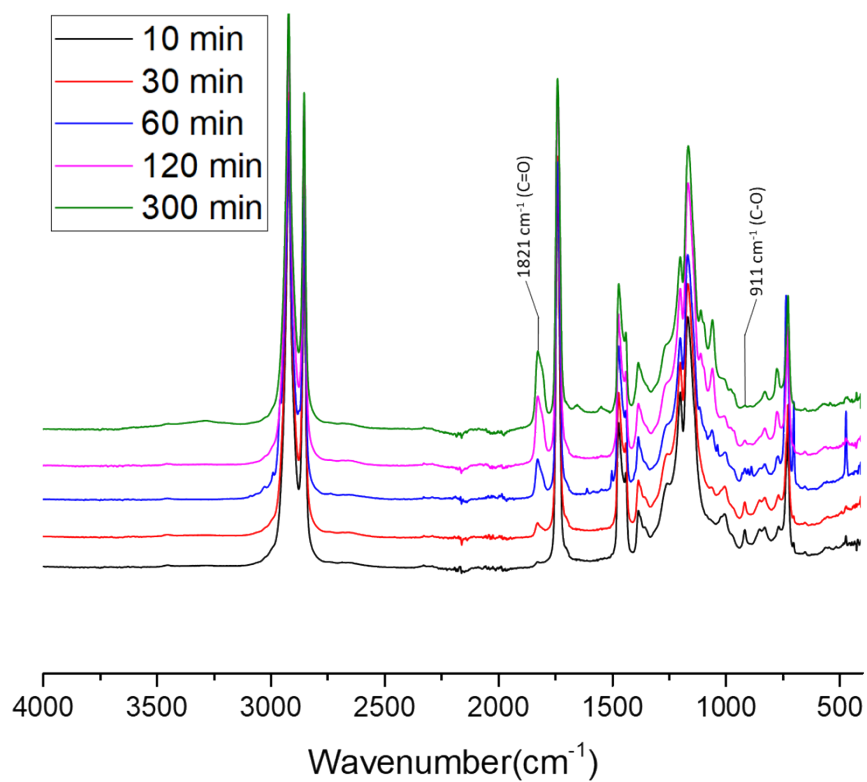
Figure S27. ATR-IR spectra of the Lotader® AX8900 modified with CO_2 (TBAI (5 mol%), 110°C, 4 MPa, toluene) for different reaction times in batch.
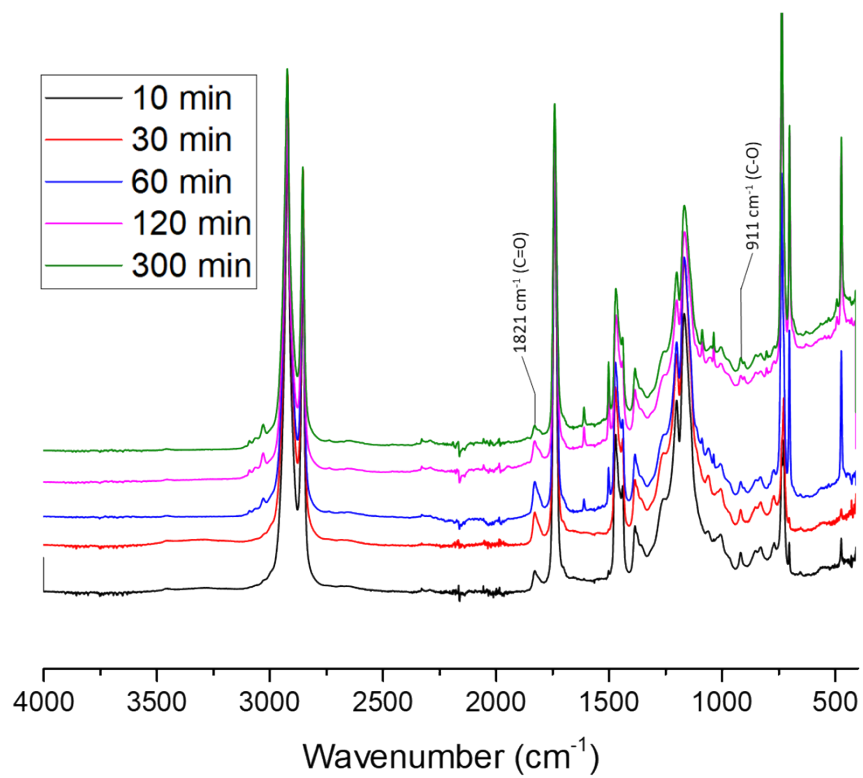
Figure S28. ATR-IR spectra of the Lotader® AX8900 modified with CO_2 (TBAC (5 mol%), 110°C, 4 MPa, toluene) for different reaction times in batch.
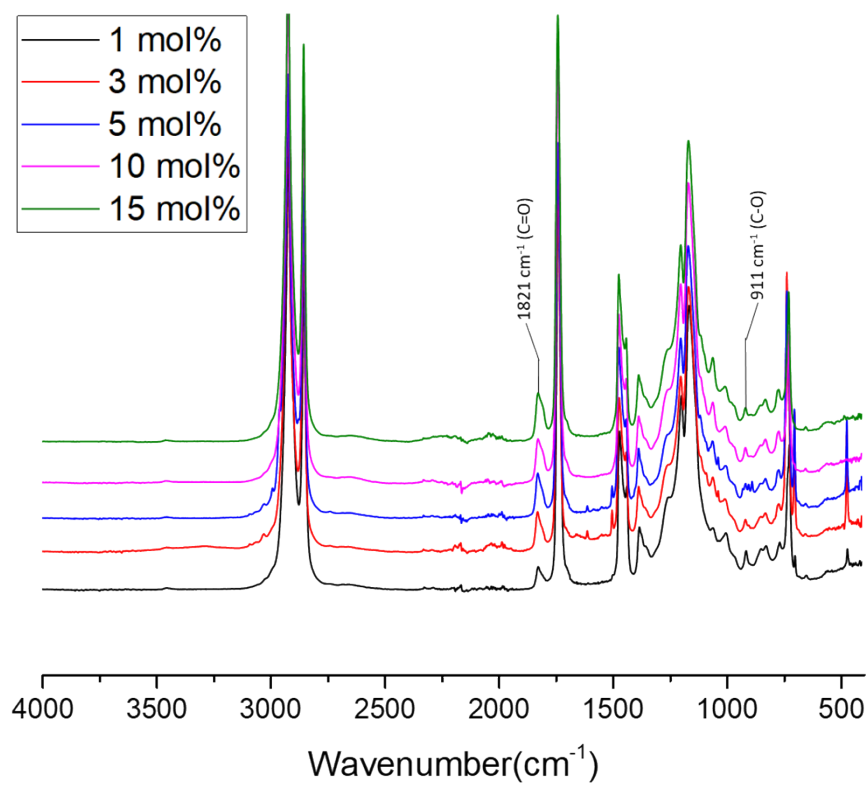
Figure S29. ATR-IR spectra of the Lotader® AX8900 modified with CO_2 (110°C, 4 MPa, toluene, 1 h) with different amounts of TBAI in batch.
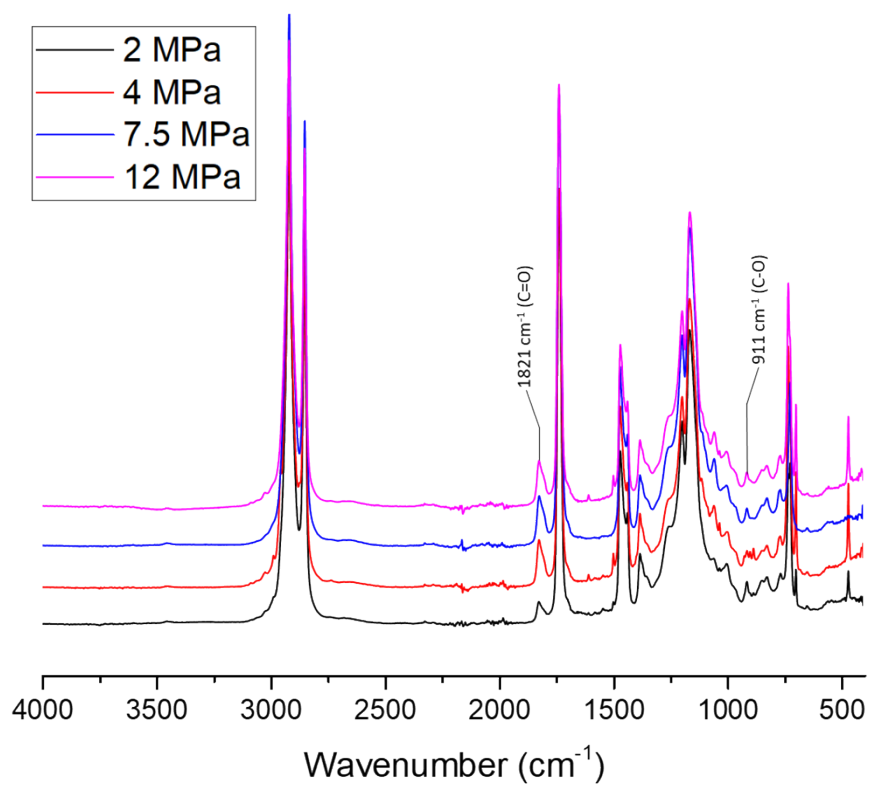
Figure S30. ATR-IR spectra of the Lotader® AX8900 modified with CO_2 (TBAI (5 mol%), 110°C, toluene, 1 h) under different pressures of CO_2 in batch.

Figure S31. ATR-IR spectra of the Lotader® AX8900 modified with CO_2 (TBAI (5 mol%), 4 MPa, toluene) at different temperatures for a reaction time of 1 h in batch.
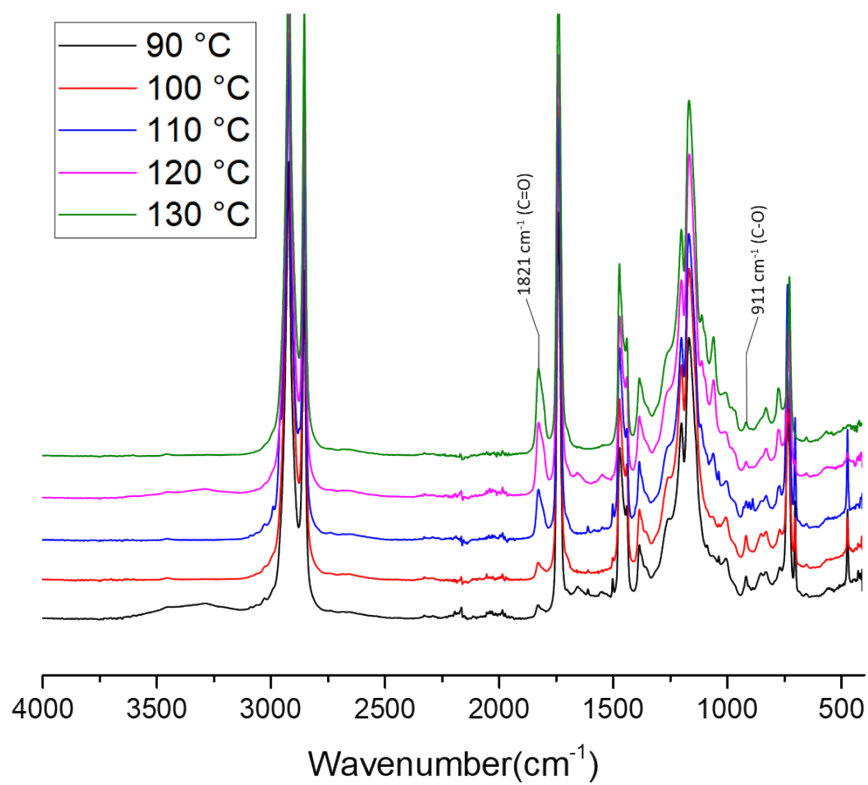
Figure S32. ATR-IR spectra of the Lotader® AX8900 modified with CO_2 (TBAI (5 mol%), 4 MPa, toluene) at different temperatures for a reaction time of 5 h in batch.
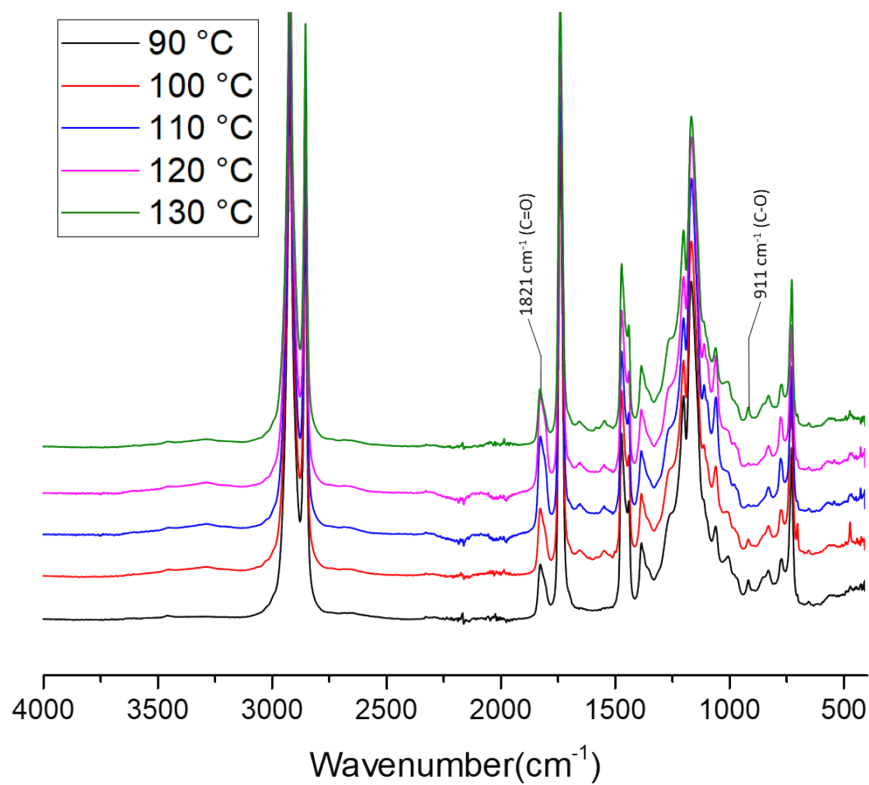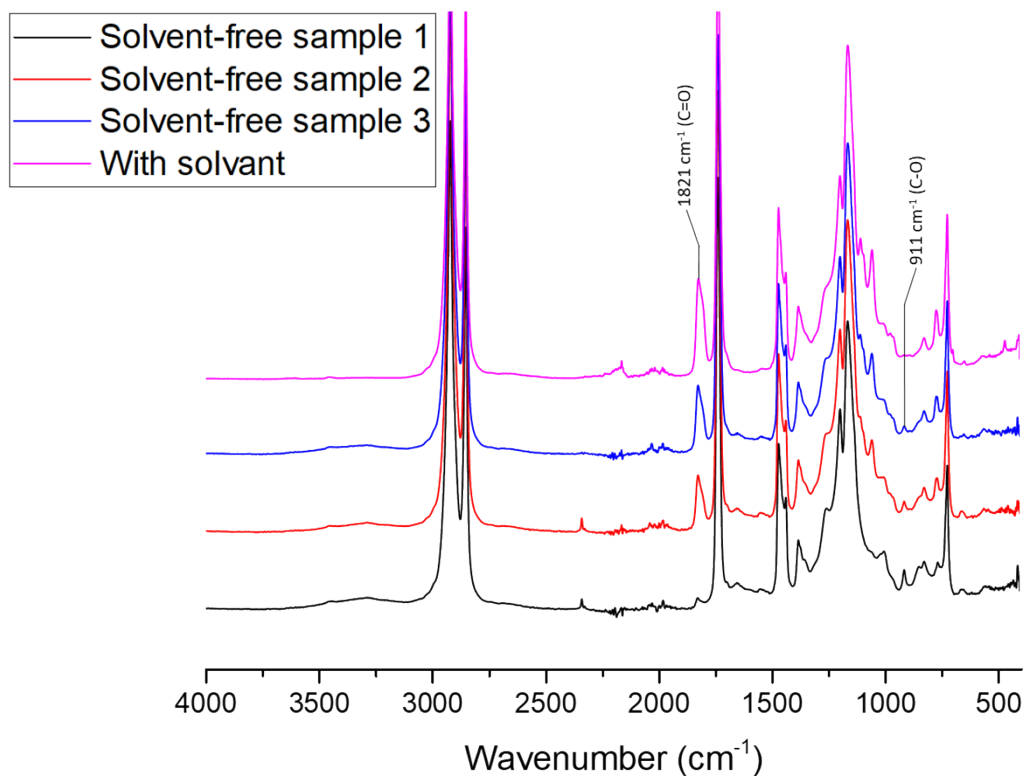
Figure S33. ATR-IR spectra of three different samples of the Lotader® AX8900 modified with CO_2 under-solvent free conditions (TBAB (5 mol%), 4 MPa of CO_2, 110 °C, 5 h). The calculated yields of sample 1, 2 and 3 are 3, 52 and 67% respectively. This experiment showcases a very heterogeneous reaction medium due to inefficient mixing of the molten polymer+catalyst under these conditions. CO_2 reactivity is thus very inhomogeneous, likely due to some dead volumes, or unreactive pockets, within the batch reactor.

Photo S1. Open Batch reactor after a reaction in the absence of solvent (toluene): observation of "pop-corning" of pellets (after decompression of CO_2) and inhomogeneous reaction medium after carbonatation reaction.
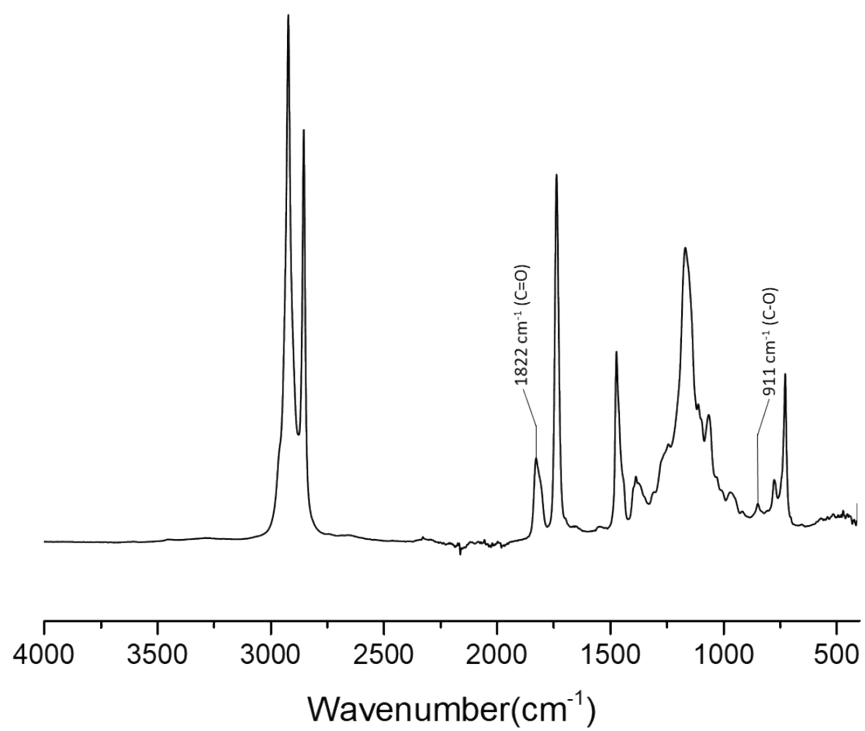
Figure S34. ATR-IR spectrum of the Lotader® AX8700 modified with CO_2 in batch.
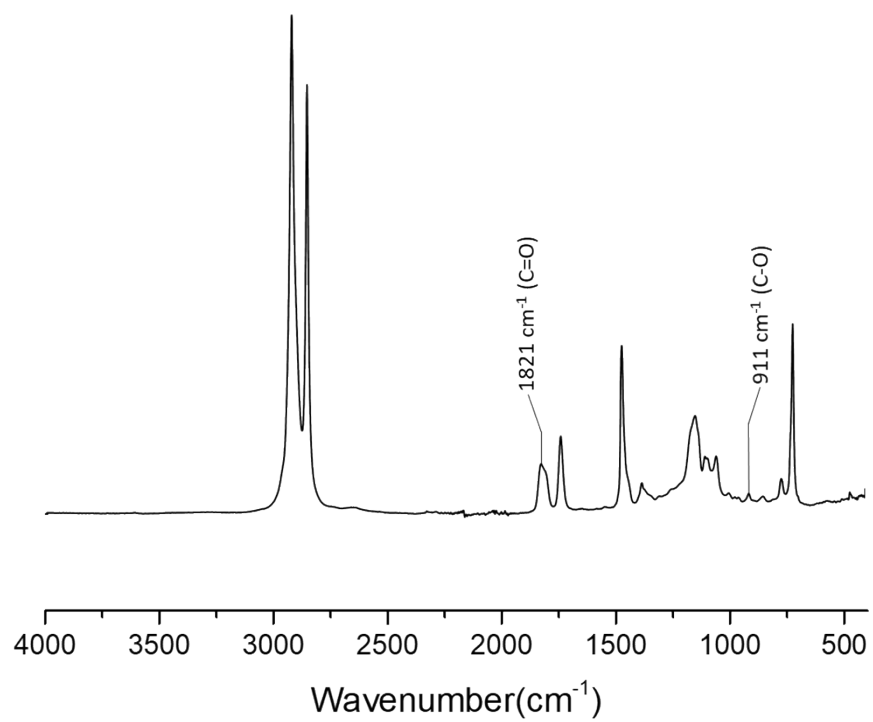
Figure S35. ATR-IR spectrum of the Lotader® AX8840 modified with CO_2 in batch.

d. <u>SEC analyses</u>

$$\log(M_n) \text{ (g/mol)}$$
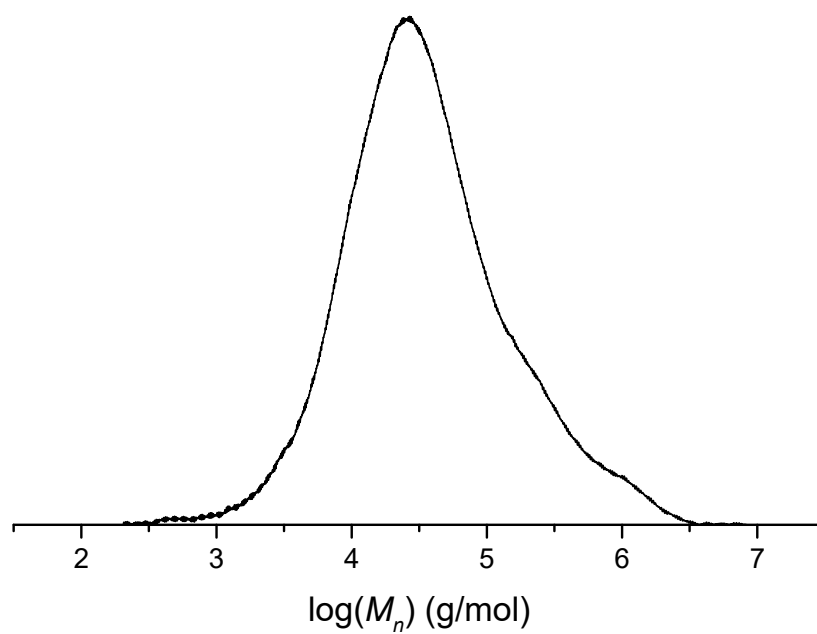
M_n	M_w
14 400	105 800

Figure S36. SEC analysis of the Lotader® AX8900 modified with CO_2 in batch.
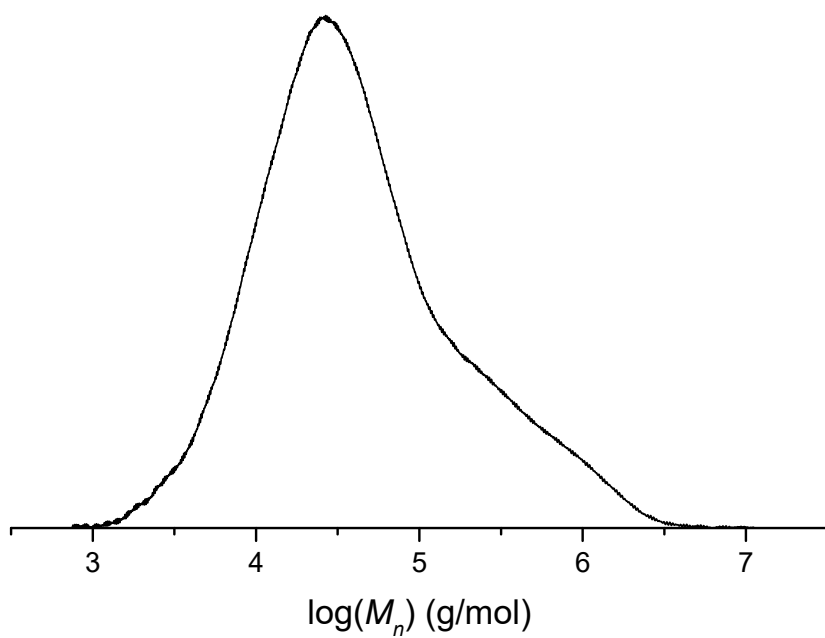
M_n	M_w
14 300	101 500

Figure S37. SEC analysis of the Lotader® AX8700 modified with CO_2 in batch.
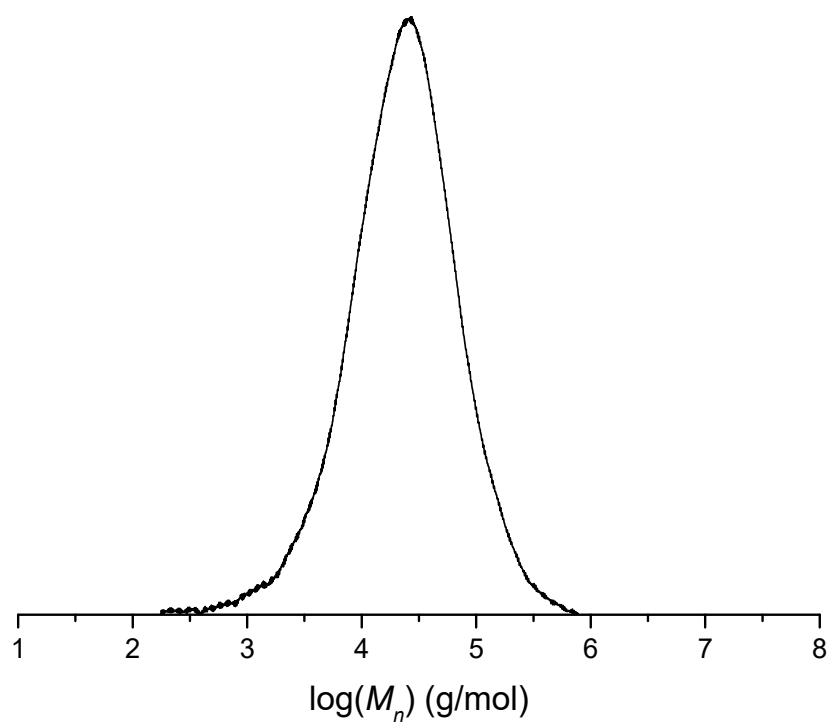
M_n	M_w
10 800	40 500

Figure S38. SEC analysis of the Lotader® AX8840 modified with CO_2 in batch.

e. DSC analyses

Figure S39. DSC analysis of the Lotader® AX8900 modified with CO_2 in batch.

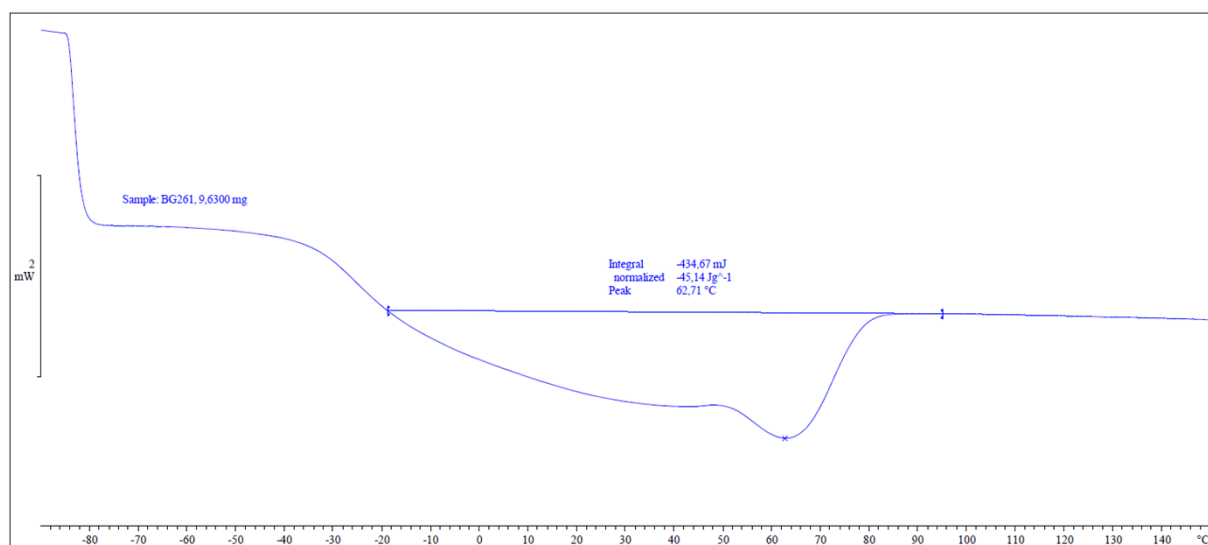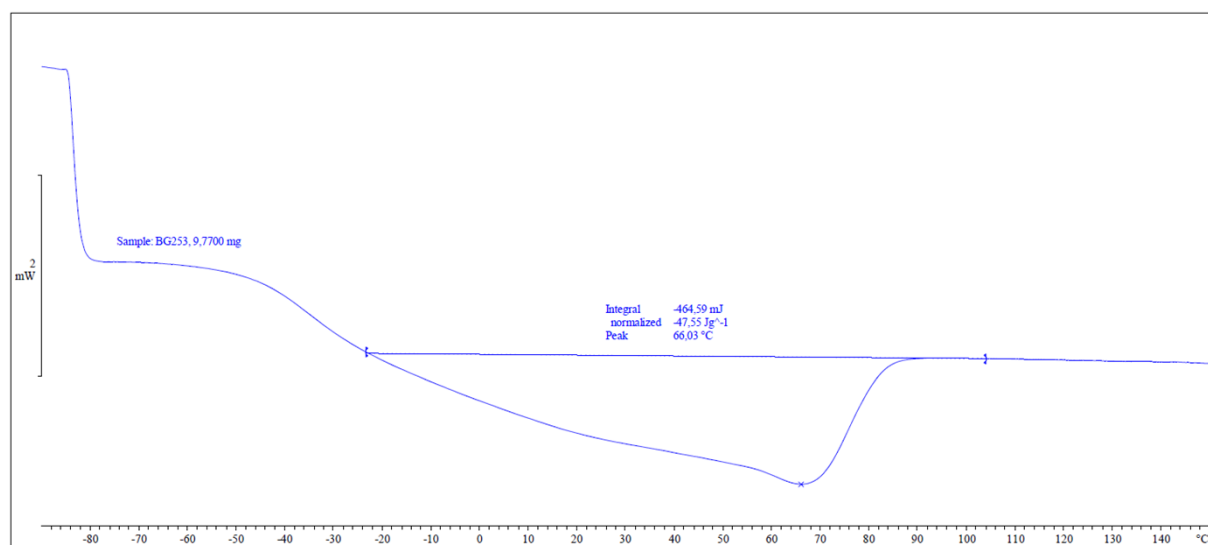**Figure S40.** DSC analysis of the Lotader® AX8700 modified with CO_2 in batch.
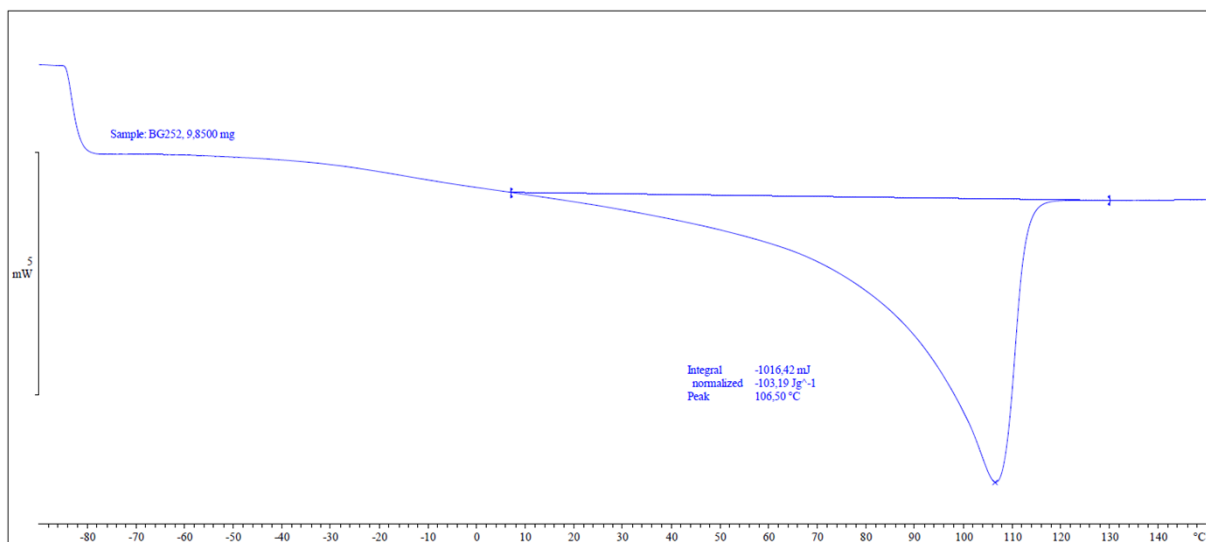
Figure S41. DSC analysis of the Lotader® AX8840 modified with CO_2 in batch.

f. TGA
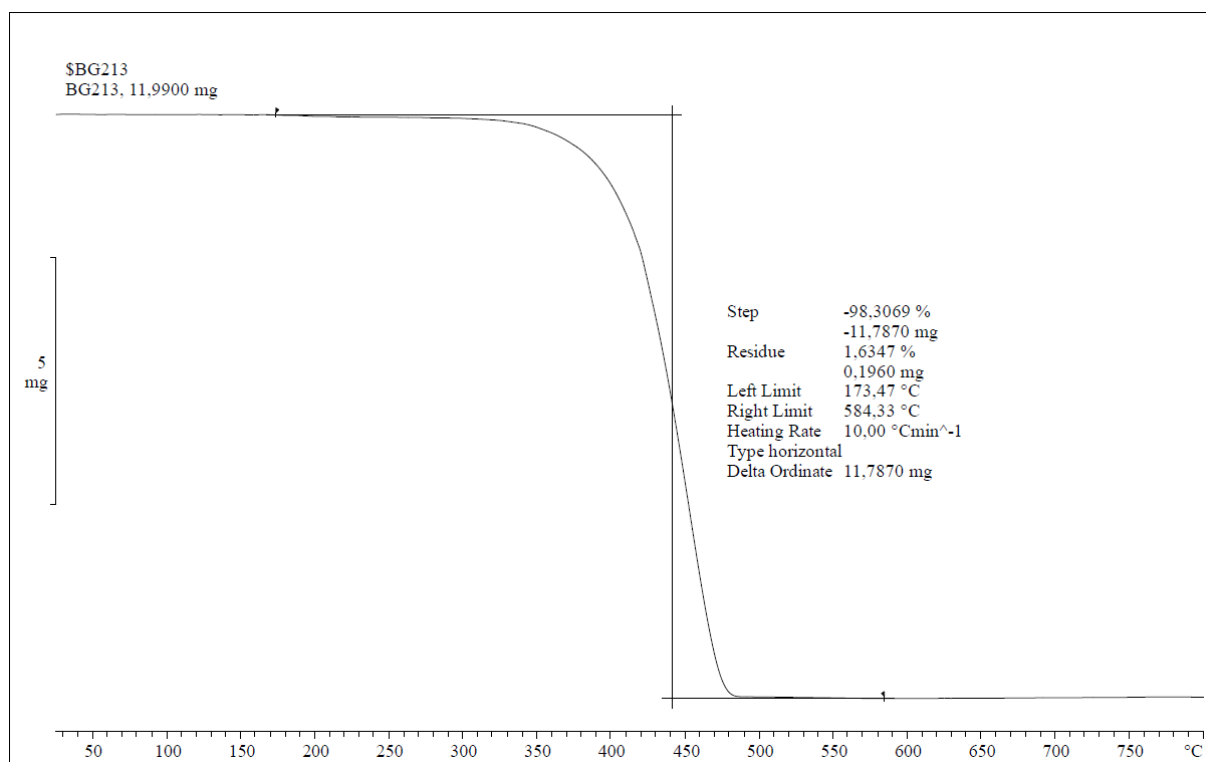
Figure S42. TGA analysis of the Lotader® AX8900 modified with CO_2 in batch.

g. <u>Rheology analysis</u>
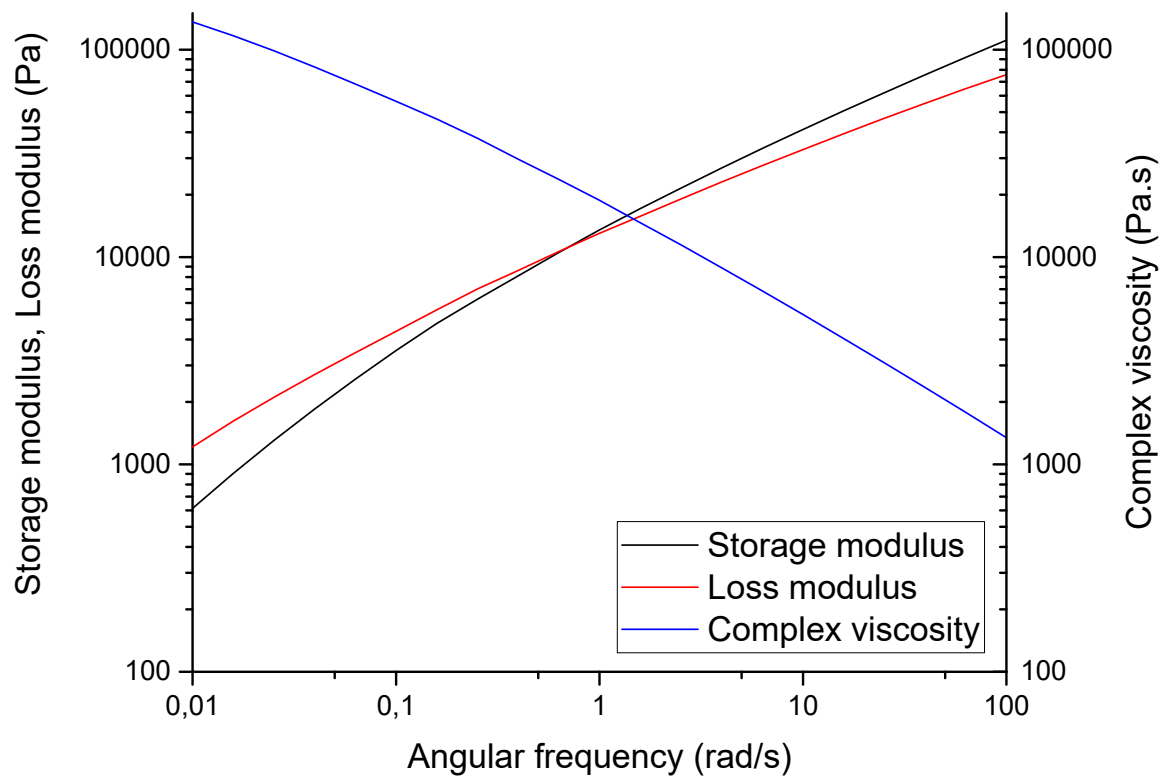
Figure S43. Rheology analysis at 150 °C of the Lotader® AX8900 modified with CO_2 in batch.

7. Characterization of the modified polymers with CO_2 in extruder

a. <u>Presentation of the reactive-extrusion process</u>
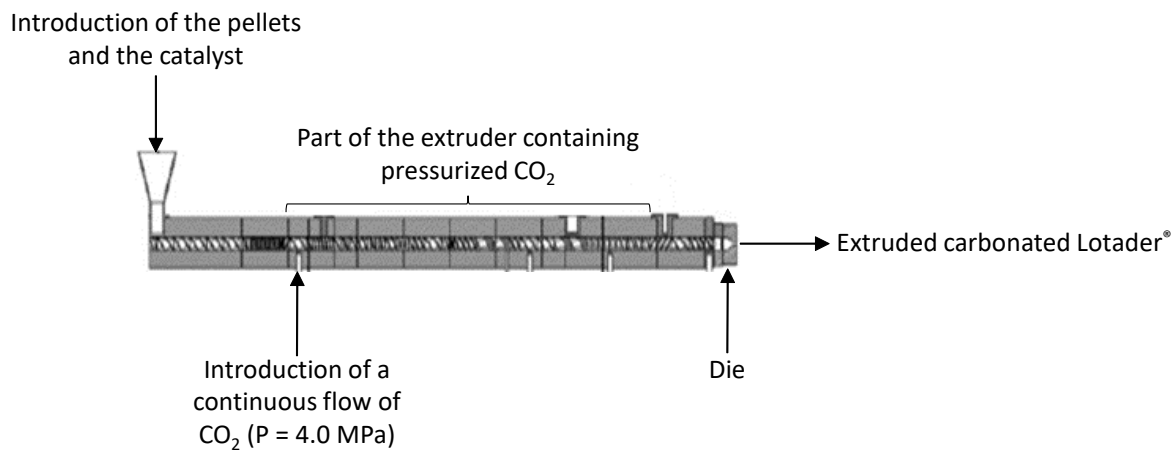
Scheme S4. Flowchart of the reactive extruder. The exact twin-screw profile is not disclosed due to IP issues.
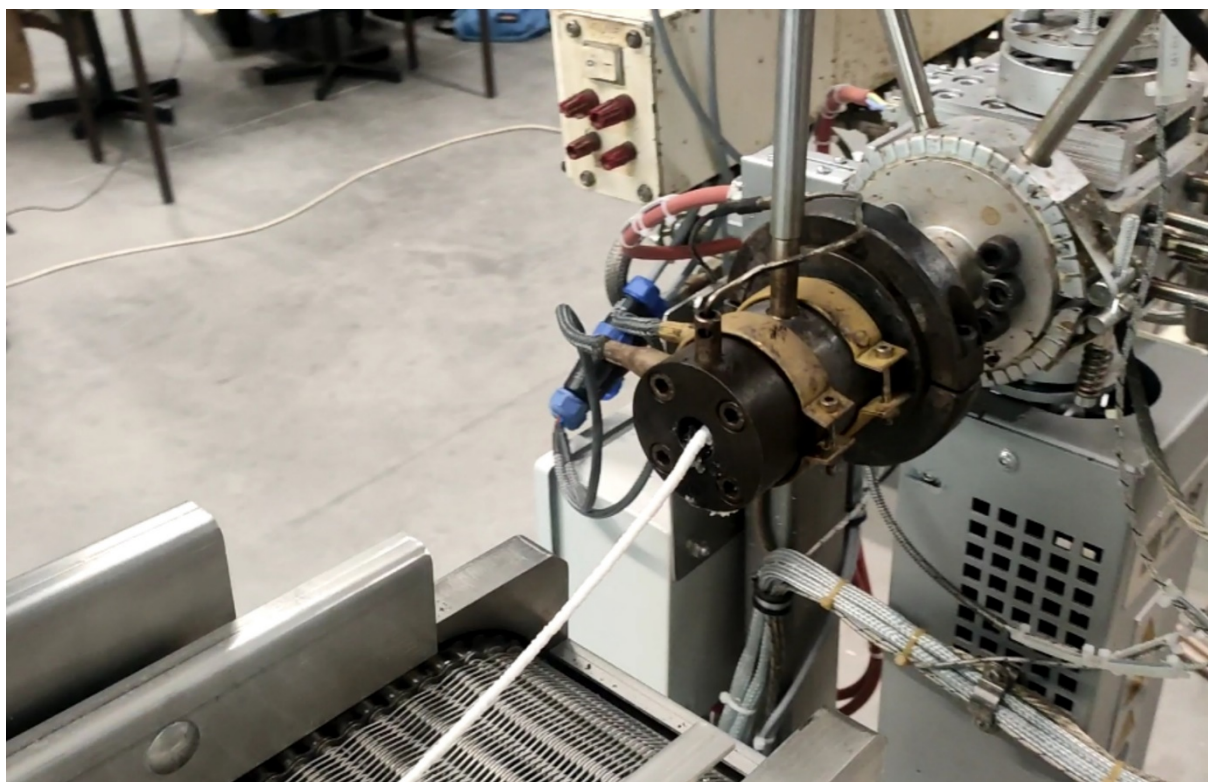
Photo S2. Reactive Extruder with carbonated Lotader® extruding from the die.

b. <u>^{1}H NMR spectra</u>

Figure S44. ^{1}H NMR (TCE/C$_6$D$_6$, 400 MHz) spectrum of the modified Lotader® AX8900 with CO$_2$ in extruder.

^{1}H NMR (400 MHz, TCE/C$_6$D$_6$) δ: 4.28 (m, g'), 4.14 (dd, J = 11.4, 2.9 Hz, f), 4.09 – 3.72 (m, f, f', h'), 3.48 (s, i) 2.90 (m, g), 2.53 – 2.21 (m, h, b), 1.88 – 0.42 (m, a, c, d, d', e, e', j, k, l).

$$Yield\ of\ cyclic\ carbonate\ = \frac{(S_{f''} + S_{g'} + S_{h'})/5}{S_g + (S_{f''} + S_{g'} + S_{h'})/5} = \frac{(14.74 - 2.00)/5}{(14.74 - 2)/5 + 1.00} = 72\ \%$$

Repeated experiment : 74%

49
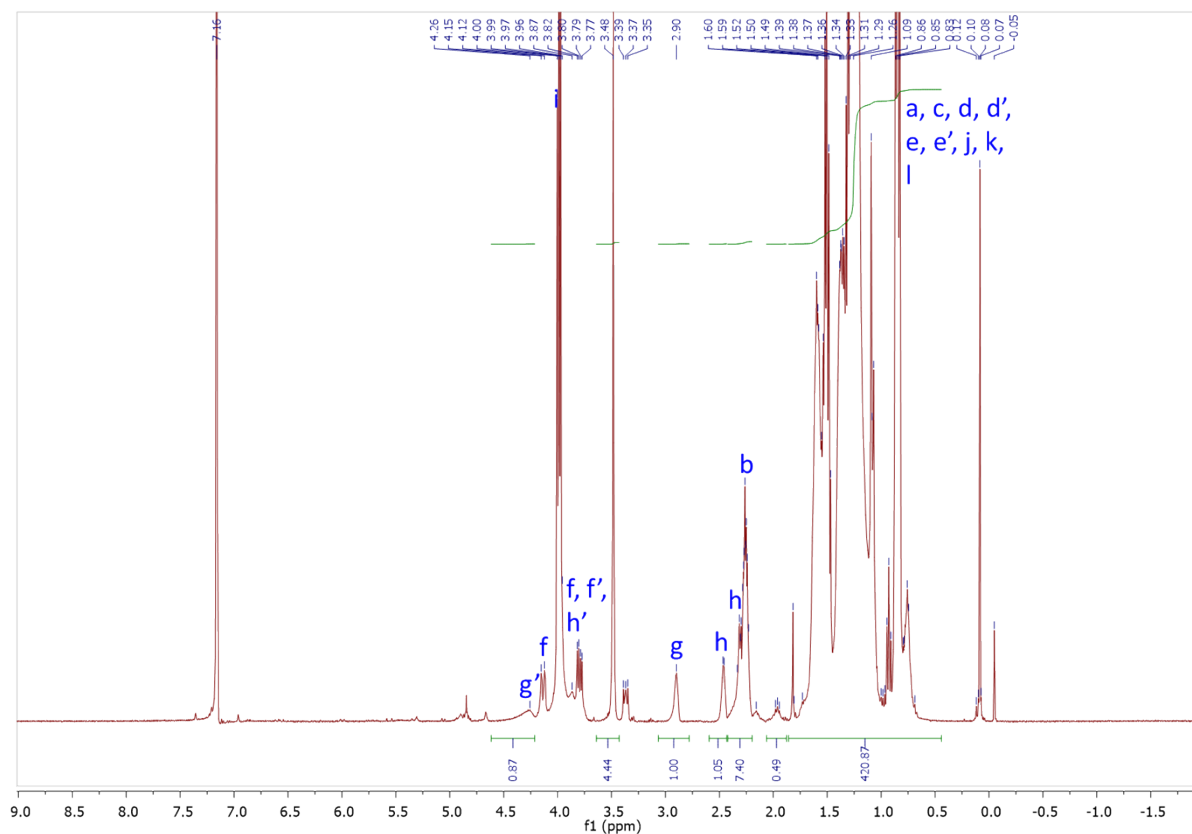
Figure S45. ^{1}H NMR (TCE/C$_6$D$_6$, 400 MHz) spectrum of the modified Lotader® AX8700 with CO$_2$ in extruder.
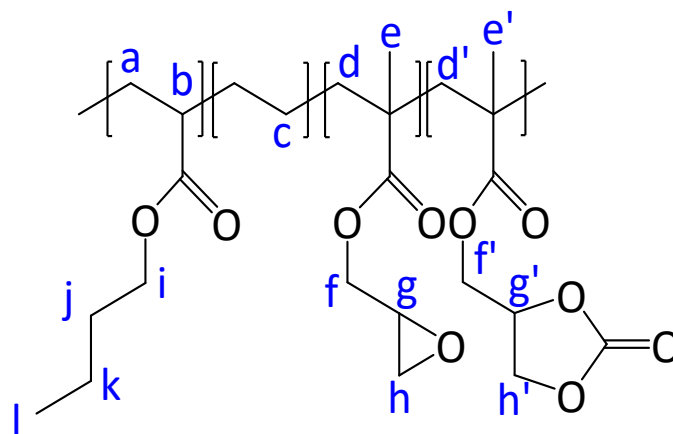
^{1}H NMR (400 MHz, TCE/C$_6$D$_6$) δ: 4.26 (m, g'), 4.14 (dd, J = 11.4, 2.9 Hz, f), 4.09 – 3.69 (m, f, f', h', i), 3,48 (methyl acrylate), 2.90 (m, g), 2.53 – 2.21 (m, h, b), 1.88 – 0.37 (m, a, c, d, d', e, e', j, k, l).

$$Yield\ of\ cyclic\ carbonate\ = \frac{S_{g'}}{S_g + S_{g'}} = \frac{0.87}{0.87 + 1.00} = 47\ \%$$
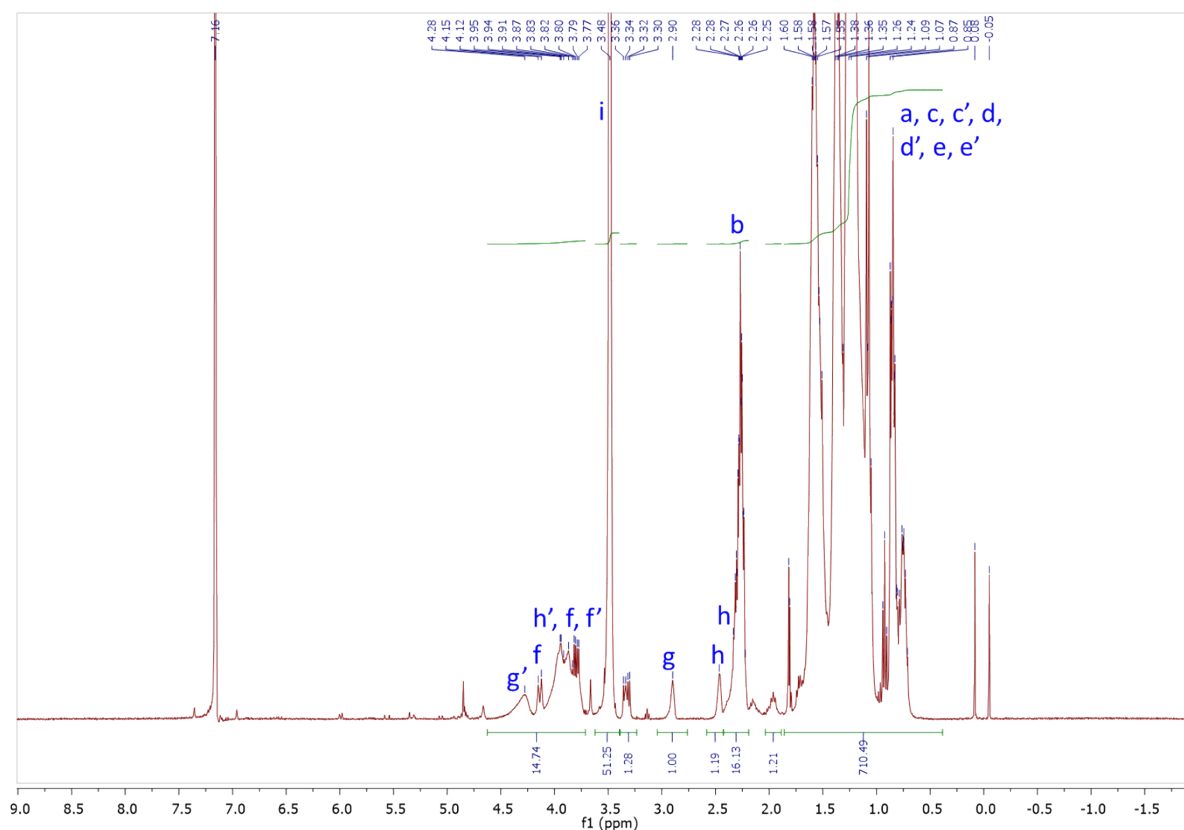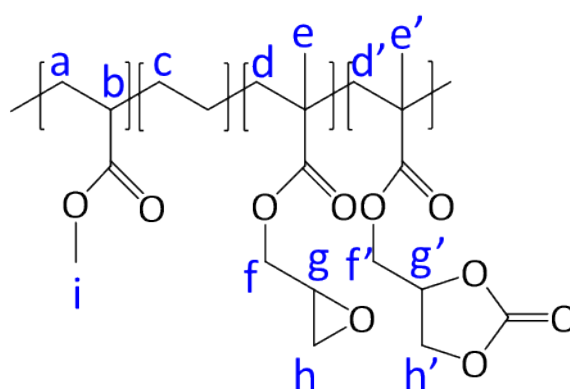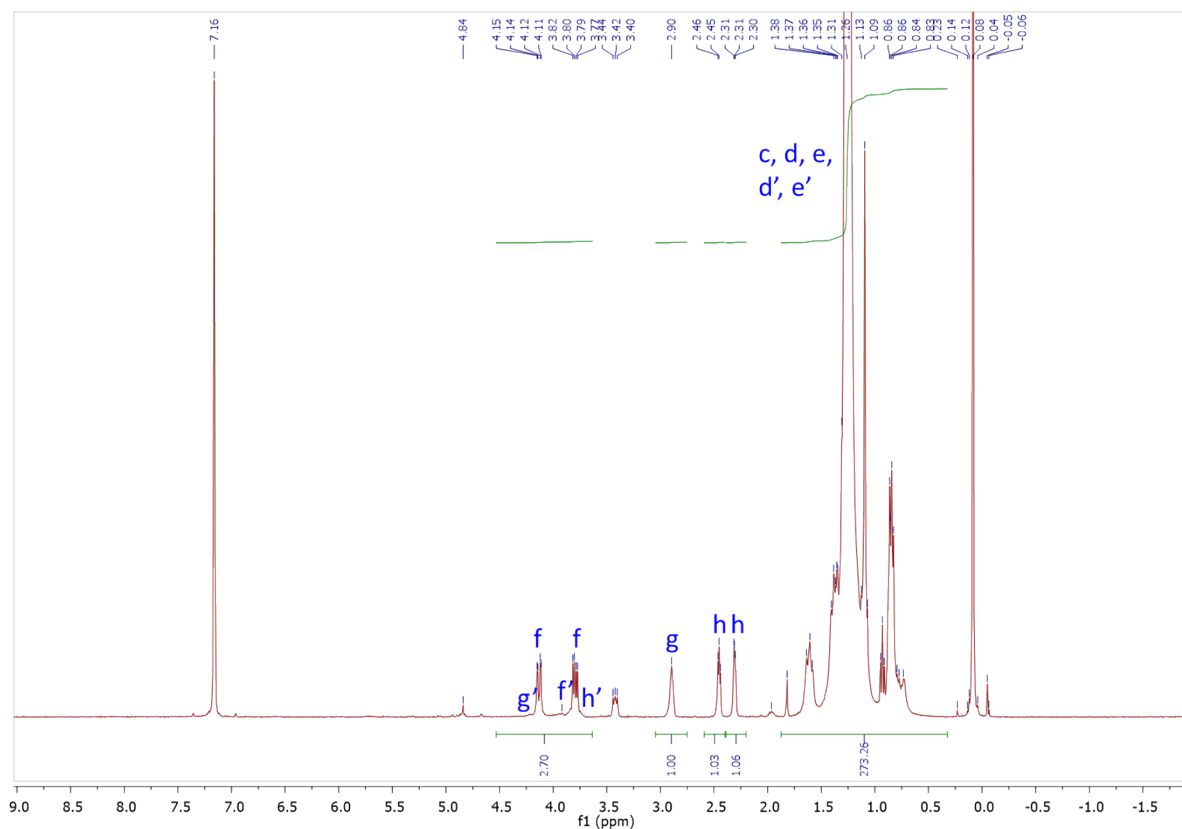
Figure S46. ^{1}H NMR (TCE/C_6D_6, 400 MHz) spectrum of the modified Lotader® AX8840 with CO_2 in extruder.
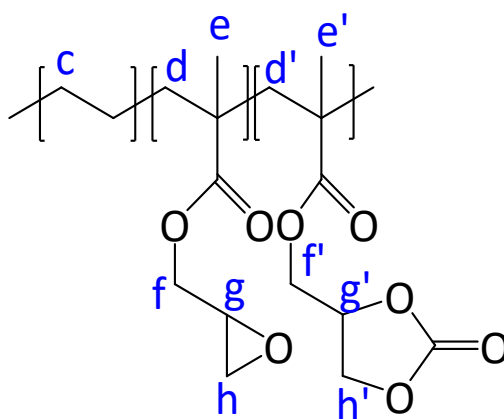
^{1}H NMR (400 MHz, TCE/C_6D_6) δ : 4.38 – 3.61 (m, f, f', g', h'), 2.90 (m, g), 2.45 (dd, J = 5.1, 4.1 Hz, h), 2.30 (dd, J = 5.3, 2.4 Hz, h), 1.88 – 0.29 (m, c, d, d', e, e').

$$Yield\ of\ cyclic\ carbonate\ = \frac{S_{f'} + S_{g'} + S_{h'}}{S_f + S_g + S_h + S_{f'} + S_{g'} + S_{h'}} = \frac{2.70 - 2 \times 1.00}{2.70 + 1.00 + 2.09} = 12\%$$

c. ATR-IR spectra
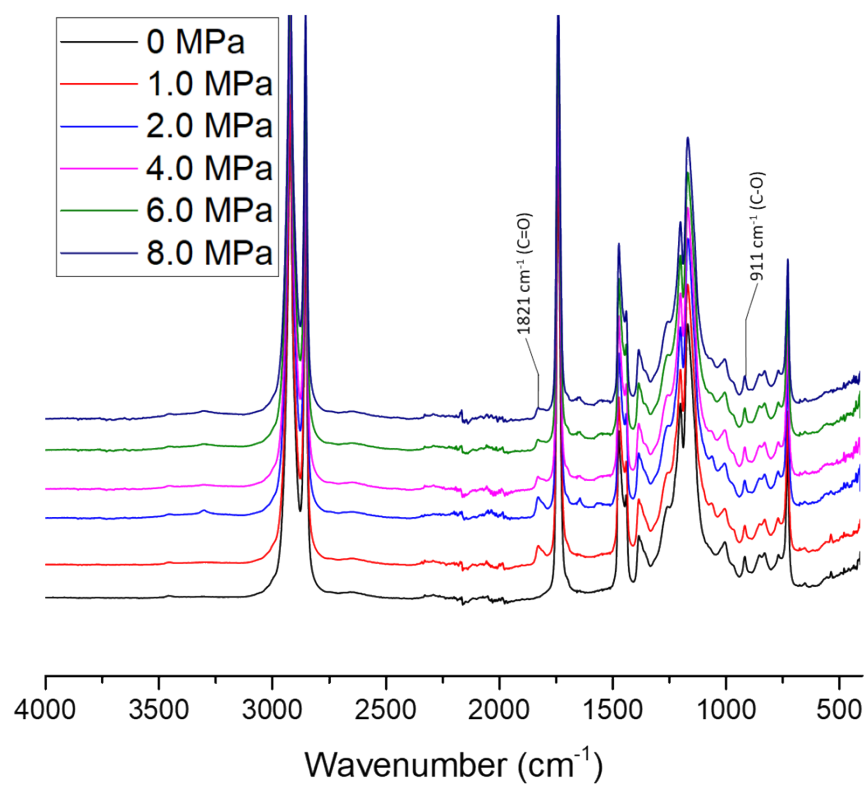
Figure S47. ATR-IR spectra of the Lotader® AX8900 modified with CO_2 (TBAB (5 mol%), 120 °C, 150 rpm, 2.0 kg/h) under different pressures of CO_2 in extruder.
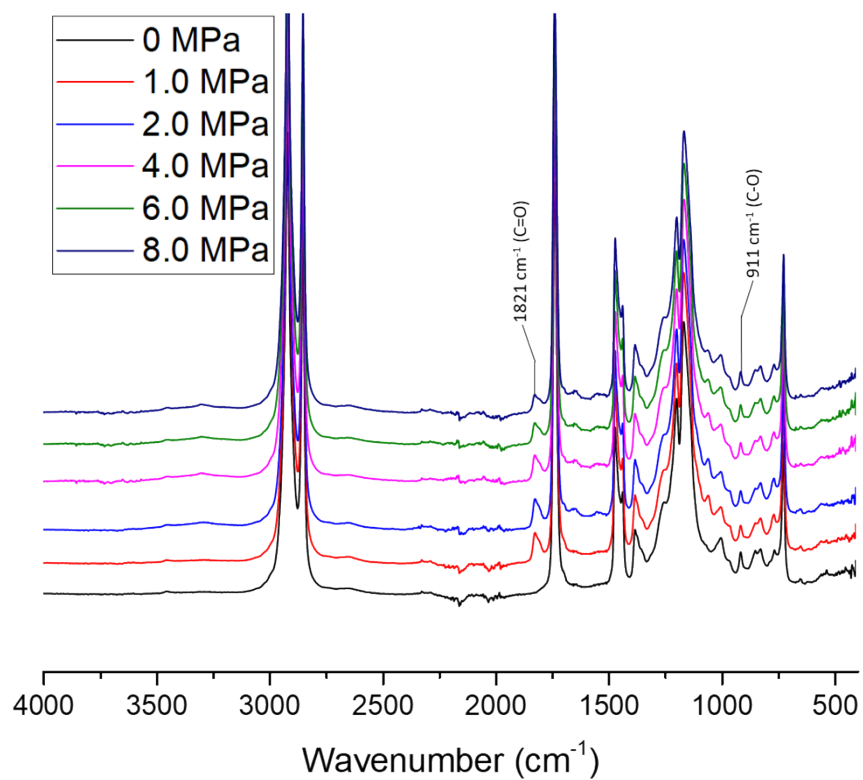
Figure S48. ATR-IR spectra of the Lotader® AX8900 modified with CO_2 (TBAB (5 mol%), 130 °C, 150 rpm, 2.0 kg/h) under different pressures of CO_2 in extruder.
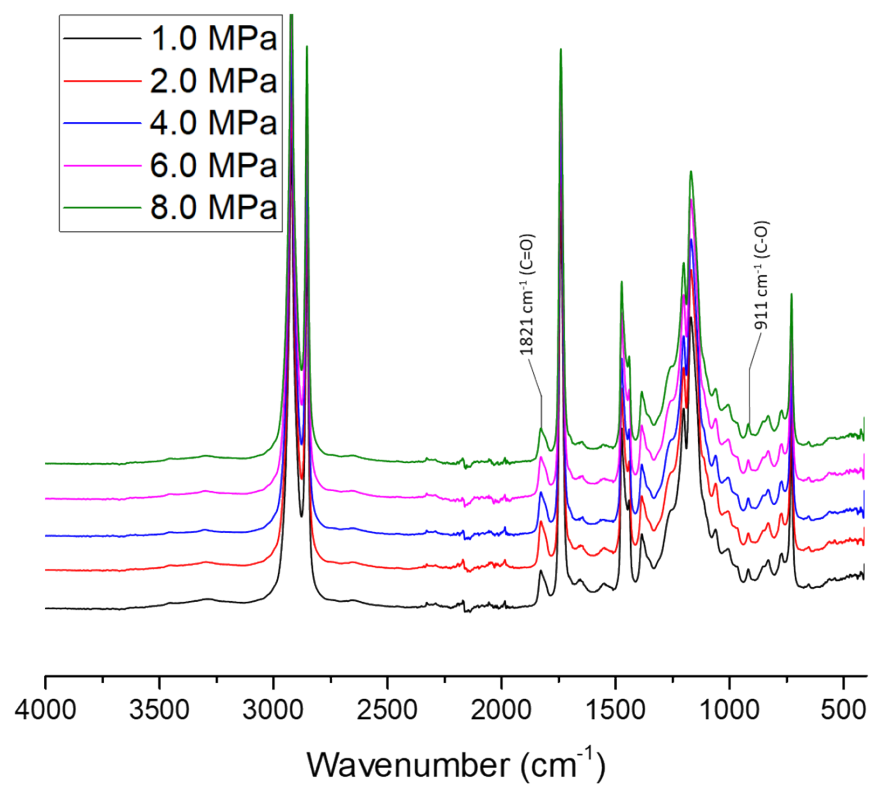
Figure S49. ATR-IR spectra of the Lotader® AX8900 modified with CO_2 (TBAB (5 mol%), 140 °C, 150 rpm, 2.0 kg/h) under different pressures of CO_2 in extruder.
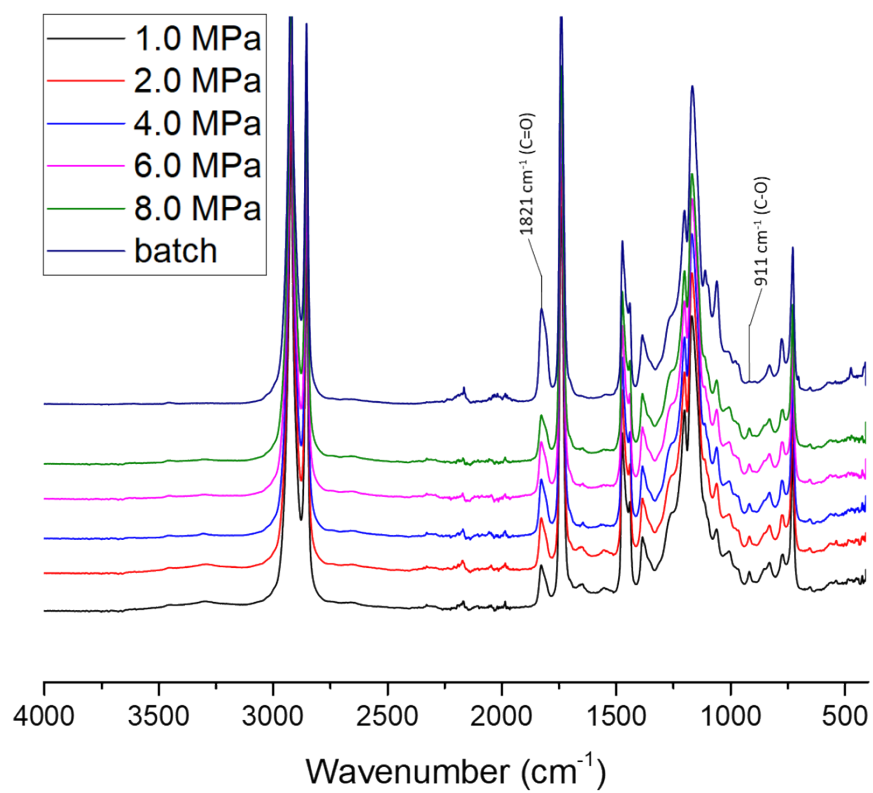
Figure S50. ATR-IR spectra of the Lotader® AX8900 modified with CO_2 (TBAB (5 mol%), 150 °C, 150 rpm, 2.0 kg/h) under different pressures of CO_2 in extruder.
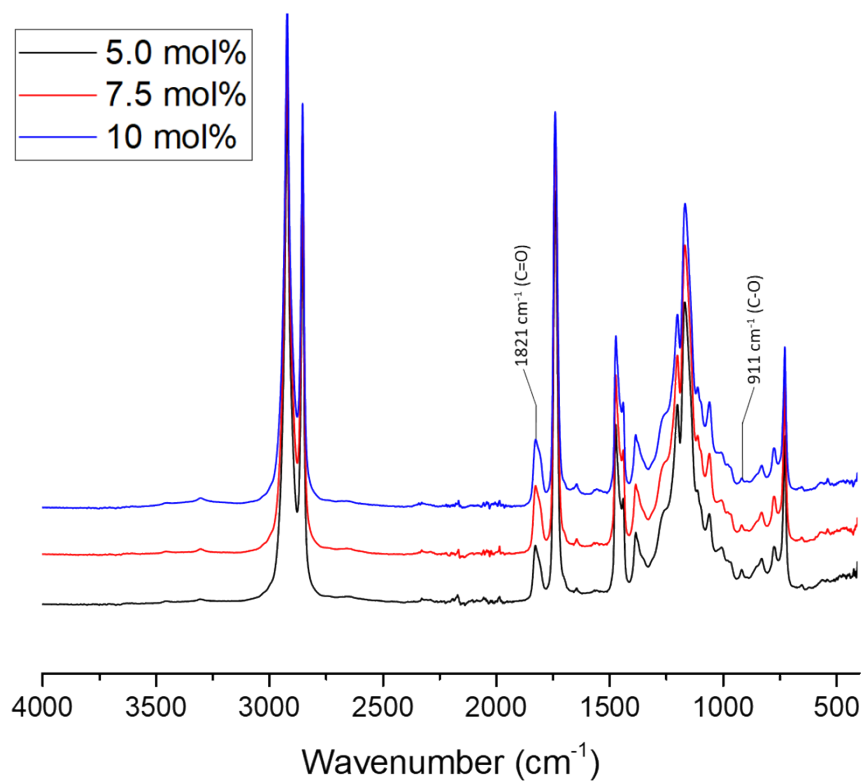
Figure S51. ATR-IR spectra of the Lotader® AX8900 modified with CO_2 (TBAB, 150 °C, 4 MPa of CO_2, 150 rpm, 2.0 kg/h) with different amounts of TBAB in extruder.
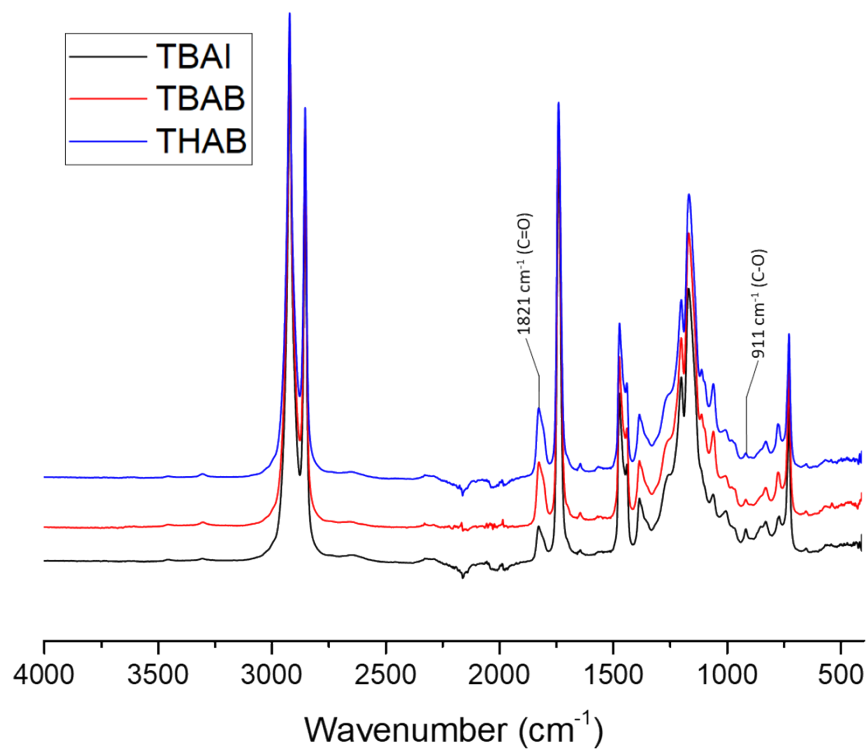
Figure S52. ATR-IR spectra of the Lotader® AX8900 modified with CO_2 (catalyst (7.5 mol%), 150 °C, 4 MPa of CO_2, 150 rpm, 2.0 kg/h) with different amounts of TBAB in extruder.
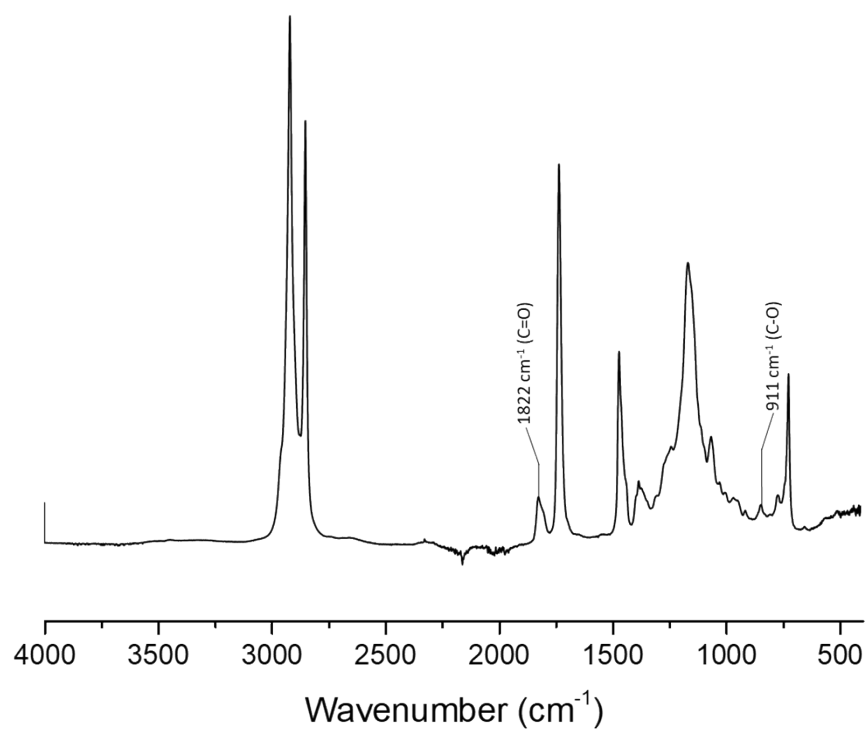
Figure S53. ATR-IR spectrum of the Lotader® AX8700 modified with CO_2 in extruder.
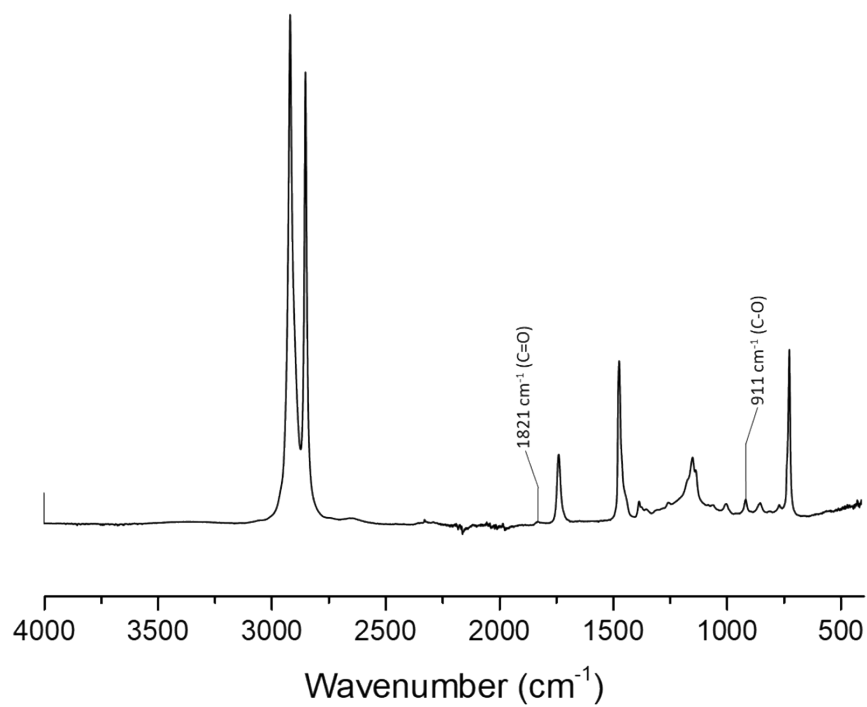
Figure S54. ATR-IR spectrum of the Lotader® AX8840 modified with CO_2 in extruder.

d. <u>SEC analyses</u>
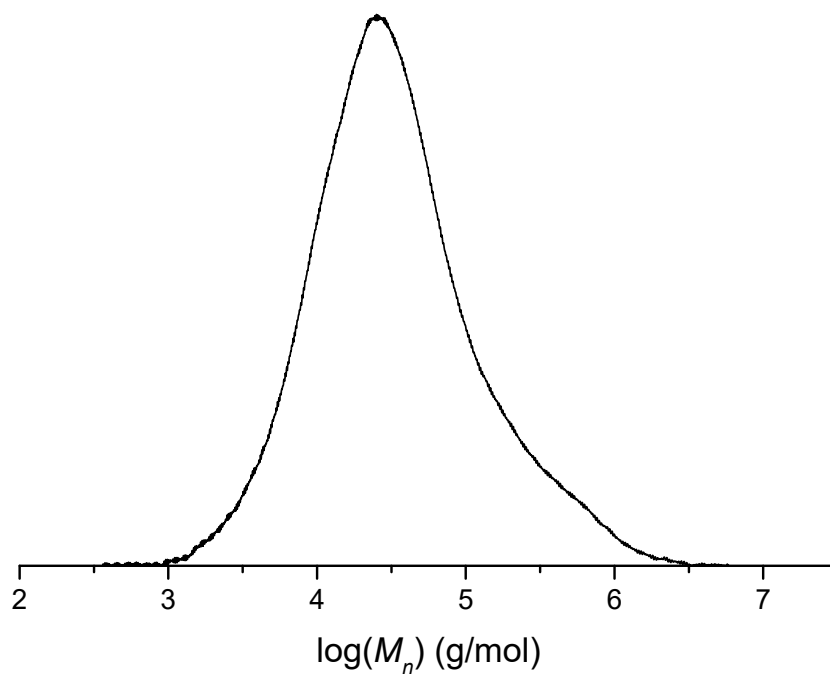
M_n	M_w
16 300	85 900

Figure S55. SEC analysis of the Lotader® AX8900 modified with CO_2 in extruder.
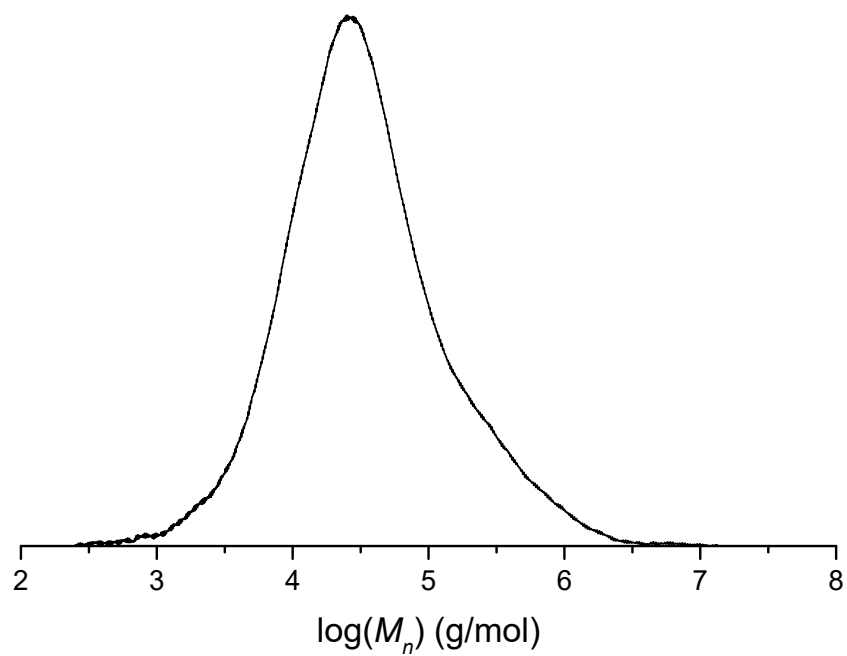
M_n	M_w
18 800	133 700

Figure S56. SEC analysis of the Lotader® AX8700 modified with CO_2 in extruder.
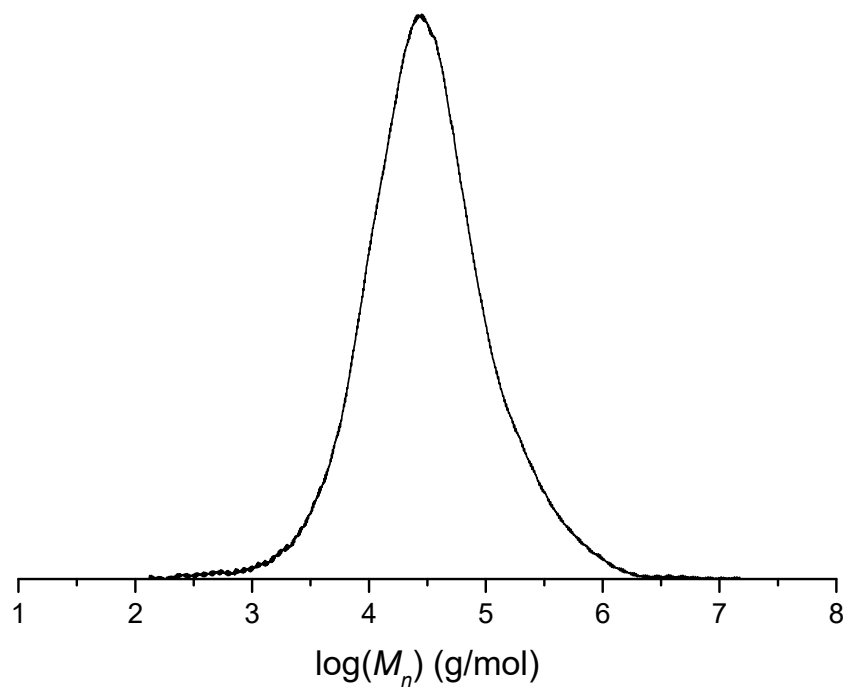
M_n	M_w
13 500	81 200

Figure S57. SEC analysis of the Lotader® AX8840 modified with CO_2 in extruder.

e. DSC analyses

Figure S58. DSC analysis of the Lotader® AX8900 modified with CO_2 in extruder.

Figure S59. DSC analysis of the Lotader® AX8700 modified with CO_2 in extruder.

63

Figure S60. DSC analysis of the Lotader® AX8840 modified with CO_2 in extruder.

8. Summary table of SEC and DSC analyses

Table S2. SEC and DSC analyses of the different Lotader® grades

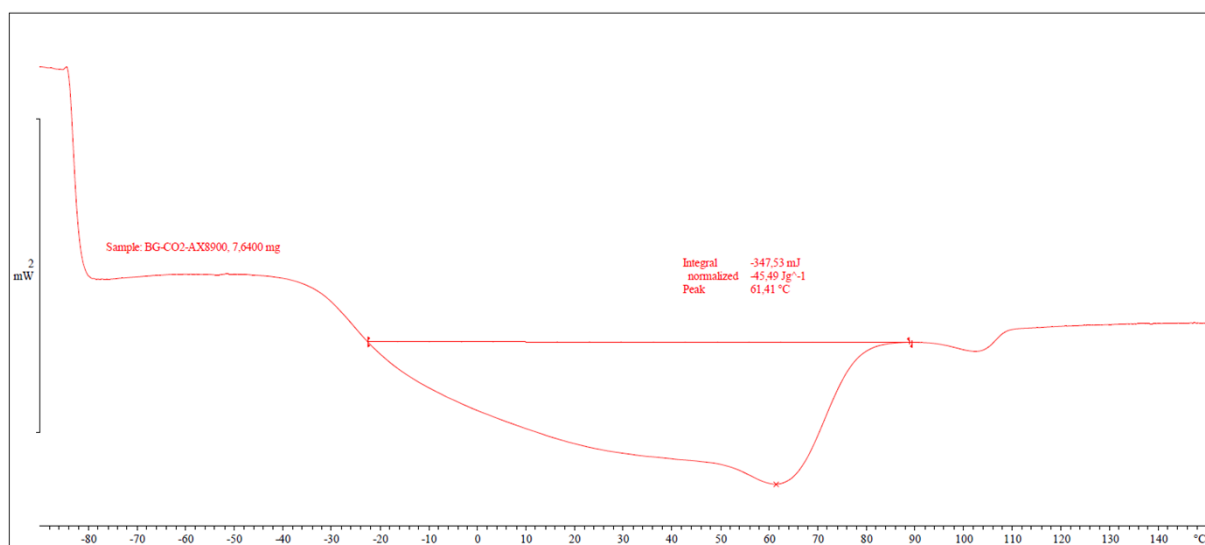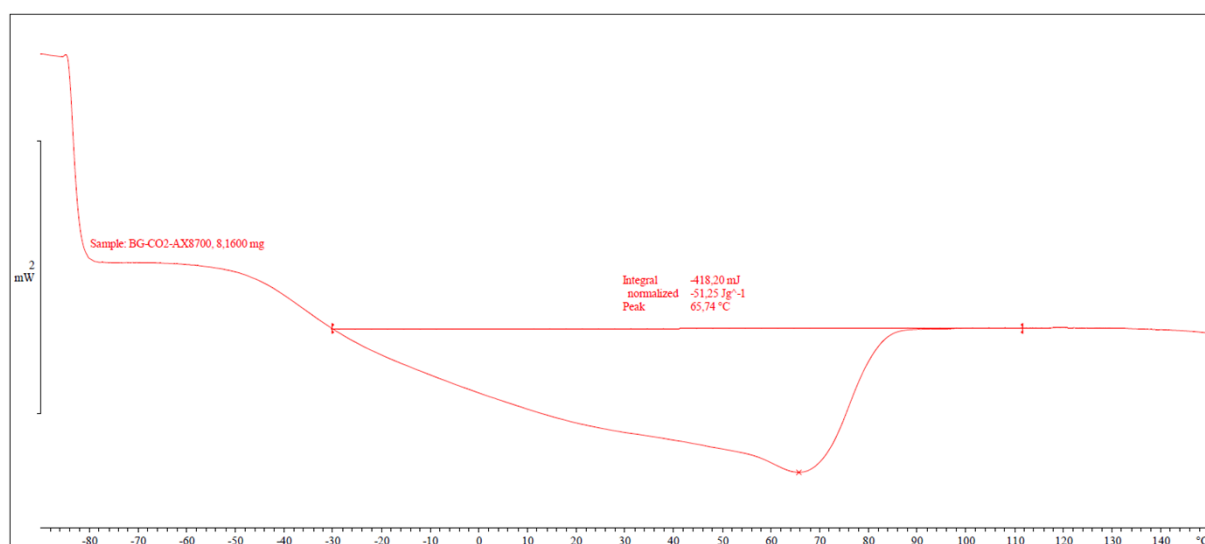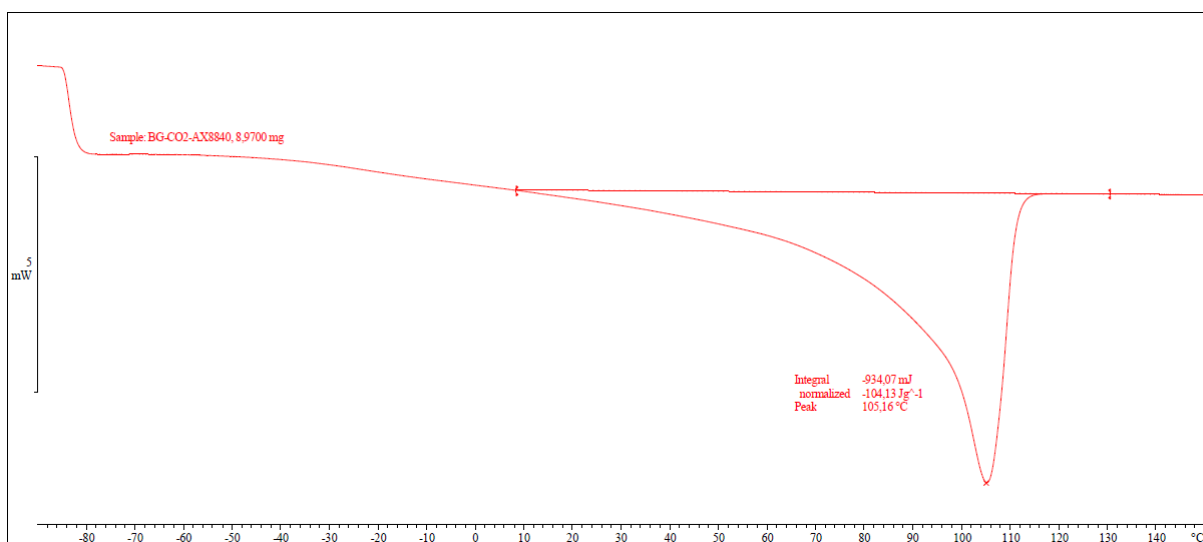| Entry	polymer	Sample	M_n (g/mol)	M_w (g/mol)	Đ	T_m (°C)
1	AX8900	1	16 600	101 300	6.1	62
2		2	16 900	84 500	5.0	
3	AX8900 modified in batch	1	14 400	105 800	7.3	63
4		2	9 600	48 800	5.1	
5	AX8900 modified in extruder	1	16 300	85 900	5.3	61
6		2	12 400	87 700	7.1	
7	AX8700	1	18 500	145 000	7.8	67
8		2	16 100	111 500	6.9	
9	AX8700 modified in batch	1	14 300	101 500	7.1	66
10		2	10 100	54 800	5.4	
11	AX8700 modified in extruder	1	18 800	133 700	7.1	66
12		2	11 700	113 600	9.7	
13	AX8840	1	17 100	55 500	3.2	105
14		2	16 500	76 600	4.6	
15	AX8840 modified in batch	1	10 800	40 500	3.8	107
16		2	12 300	100 900	8.2	
17	AX8840 modified in extruder	1	13 500	81 200	6.0	105
18		2	15 300	106 400	7.0	

High values of dispersities Đ are common for LDPE and LDPE-based copolymers synthesized using high temperatures (typically >200°C) and high pressures (>1500 bar, up to 3000 bar): see for instance Ref [29]. Some variations in M_w can be observed even in the native Lotader® grades, from sample to sample, and some chain scissions/radical coupling can occur due to prolonged shear stress, in particular in the batch processes with extensive mechanical stirring, albeit to a very reasonable extent.
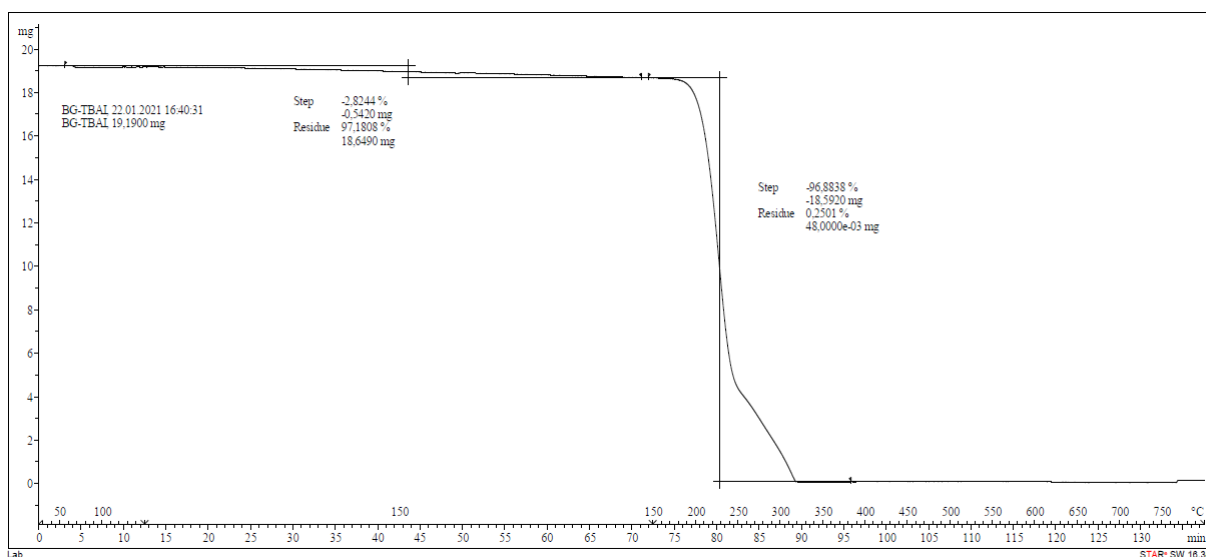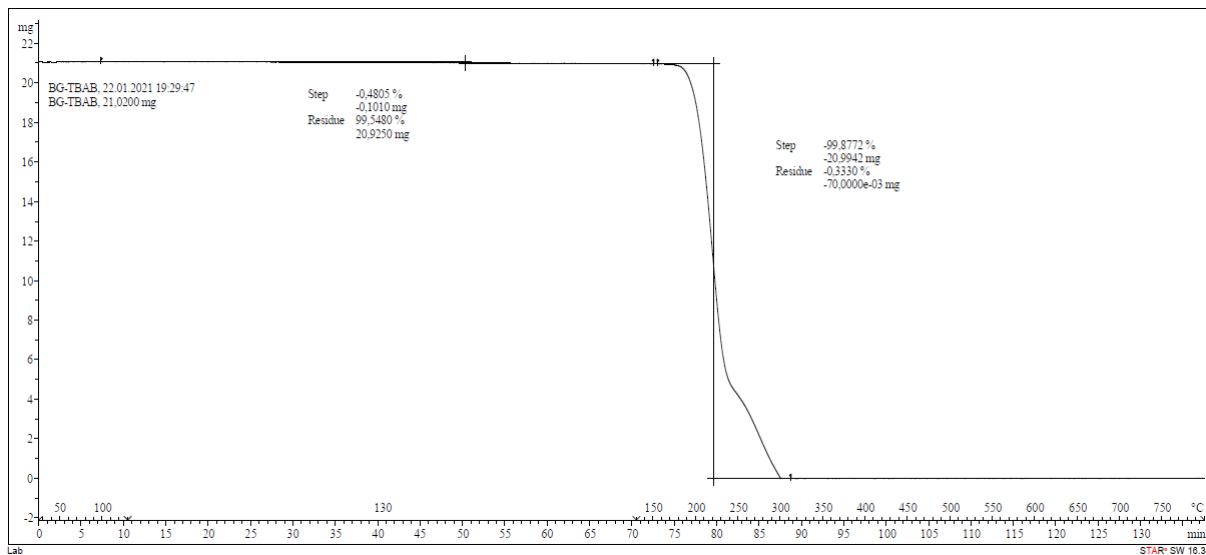
9. TGA of the catalysts

Figure S61. TGA of TBAI.
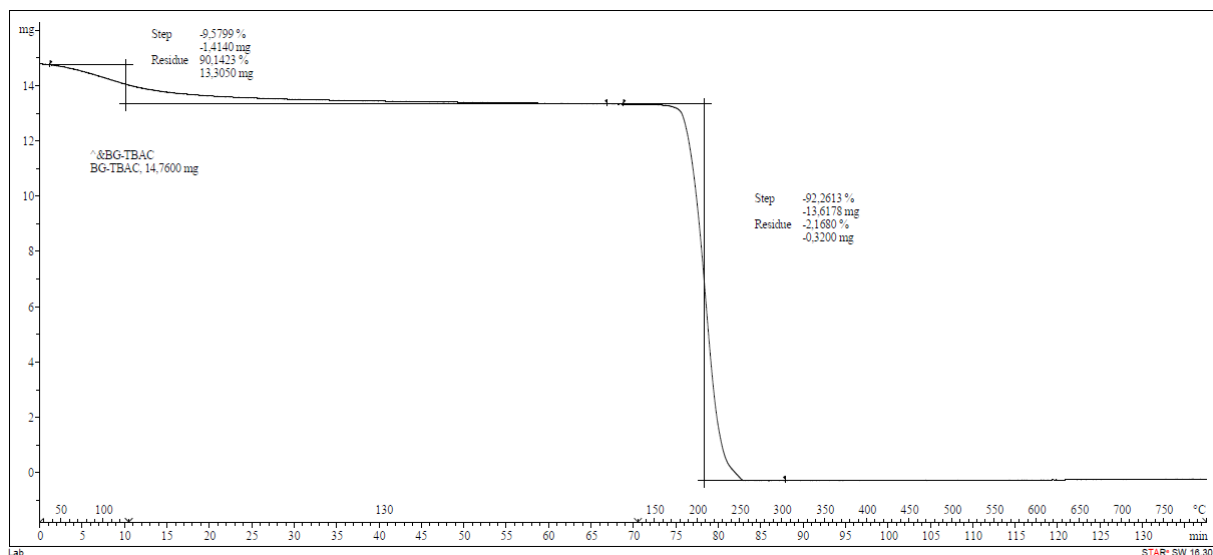

Figure S62. TGA of TBAB.

Figure S63. TGA of TBAC.

10. References

1   V. Caló, A. Nacci, A. Monopoli and A. Fanizzi, *Org. Lett.*, 2002, **4**, 2561–2563.

2   H. Kim, *Journal of Catalysis*, 2003, **220**, 44–46.

3   D. J. Darensbourg, S. J. Lewis, J. L. Rodgers and J. C. Yarbrough, *Inorg. Chem.*, 2003, **42**, 581–589.

4   J. Sun, S.-I. Fujita, F. Zhao and M. Arai, *Applied Catalysis A: General*, 2005, **287**, 221–226.

5   H. Sugimoto and K. Kuroda, *Macromolecules*, 2008, **41**, 312–317.

6   A. Sibaouih, P. Ryan, M. Leskelä, B. Rieger and T. Repo, *Applied Catalysis A: General*, 2009, **365**, 194–198.

7   D. J. Darensbourg and A. I. Moncada, *Macromolecules*, 2010, **43**, 5996–6003.

8   X.-B. Lu and D. J. Darensbourg, *Chem. Soc. Rev.*, 2012, **41**, 1462–1484.

9   D. Tian, B. Liu, Q. Gan, H. Li and Donald. J. Darensbourg, *ACS Catal.*, 2012, **2**, 2029–2035.

10 Y. Yang, Y. Hayashi, Y. Fujii, T. Nagano, Y. Kita, T. Ohshima, J. Okuda and K. Mashima, *Catal. Sci. Technol.*, 2012, **2**, 509–513.

11 C. J. Whiteoak, N. Kielland, V. Laserna, F. Castro-Gómez, E. Martin, E. C. Escudero-Adán, C. Bo and A. W. Kleij, *Chem. Eur. J.*, 2014, **20**, 2264–2275.

12 J. Rintjema and A. W. Kleij, *ChemSusChem*, 2017, **10**, 1274–1282.

13 D. O. Meléndez, A. Lara-Sánchez, J. Martínez, X. Wu, A. Otero, J. A. Castro-Osma, M. North and R. S. Rojas, *ChemCatChem*, 2018, **10**, 2271–2277.

14 Q. Yao, Y. Shi, Y. Wang, X. Zhu, D. Yuan and Y. Yao, *Asian Journal of Organic Chemistry*, 2022, **11**, e202200106.

15 B. Chatelet, L. Joucla, J.-P. Dutasta, A. Martinez, K. C. Szeto and V. Dufaud, *J. Am. Chem. Soc.*, 2013, **135**, 5348–5351.

16 S. Gennen, M. Alves, R. Méreau, T. Tassaing, B. Gilbert, C. Detrembleur, C. Jerome and B. Grignard, *ChemSusChem*, 2015, **8**, 1845–1849.

17 S. Arayachukiat, C. Kongtes, A. Barthel, S. V. C. Vummaleti, A. Poater, S. Wannakao, L. Cavallo and V. D'Elia, *ACS Sustainable Chem. Eng.*, 2017, **5**, 6392–6397.

18 Á. Mesías-Salazar, J. Martínez, R. S. Rojas, F. Carrillo-Hermosilla, A. Ramos, R. Fernández-Galán and A. Antiñolo, *Catal. Sci. Technol.*, 2019, **9**, 3879–3886.

19 H. Ma, J. Zeng, D. Tu, W. Mao, B. Zhao, K. Wang, Z. Liu and J. Lu, *Tetrahedron Letters*, 2020, **61**, 151593.

20 H. Kawanami, A. Sasaki, K. Matsui and Y. Ikushima, *Chem. Commun.*, 2003, 896–897.

21 T. Seki, J.-D. Grunwaldt and A. Baiker, *J. Phys. Chem. B*, 2009, **113**, 114–122.

22 W. Natongchai, J. A. Luque-Urrutia, C. Phungpanya, M. Solà, V. D'Elia, A. Poater and H. Zipse, *Org. Chem. Front.*, 2021, **8**, 613–627.

23 M. A. Fuchs, T. A. Zevaco, E. Ember, O. Walter, I. Held, E. Dinjus and M. Döring, *Dalton Trans.*, 2013, **42**, 5322.

24 M. Hong, Y. Kim, H. Kim, H. J. Cho, M.-H. Baik and Y. Kim, *J. Org. Chem.*, 2018, **83**, 9370–9380.

25 T. Ema, Y. Miyazaki, S. Koyama, Y. Yano and T. Sakai, *Chem. Commun.*, 2012, **48**, 4489.

26 T. Chang, L. Jin and H. Jing, *ChemCatChem*, 2009, **1**, 379–383.

27 T. Werner and H. Büttner, *ChemSusChem*, 2014, **7**, 3268–3271.

28 K. Hatada, T. Kitayama, K. Ute, Y. Terawaki and T. Yanagida, *Macromolecules*, 1997, **30**, 6754–6759.

29 K. M. Zentel, P. S. E. Bungu, H. Pasch and M. Busch, *Polym. Chem.*, 2021, **12**, 3026–3041.